

# Overcoming Preclinical Safety Obstacles to Discover (*S*)-*N*-((1,2,3,5,6,7-Hexahydro-*s*-indacen-4-yl)carbamoyl)-6-(methylamino)-6,7-dihydro-5*H*-pyrazolo[5,1-*b*][1,3]oxazine-3-sulfonamide (GDC-2394): A Potent and Selective NLRP3 Inhibitor

Christopher McBride, Lynnie Trzoss, Davide Povero, Milos Lazic, Geza Ambrus-Aikelin, Angelina Santini, Rama Pranadinata, Gretchen Bain, Ryan Stansfield, Jeffrey A. Stafford, James Veal, Ryan Takahashi, Justin Ly, Shu Chen, Liling Liu, Marika Nespi, Robert Blake, Arna Katewa, Tracy Kleinheinz, Swathi Sujatha-Bhaskar, Nandhini Ramamoorthi, Jessica Sims, Brent McKenzie, Mark Chen, Mark Ultsch, Matthew Johnson, Jeremy Murray, Claudio Ciferri, Steven T. Staben, Michael J. Townsend,\* and Craig E. Stivala\*



Cite This: <https://doi.org/10.1021/acs.jmedchem.2c01250>



Read Online

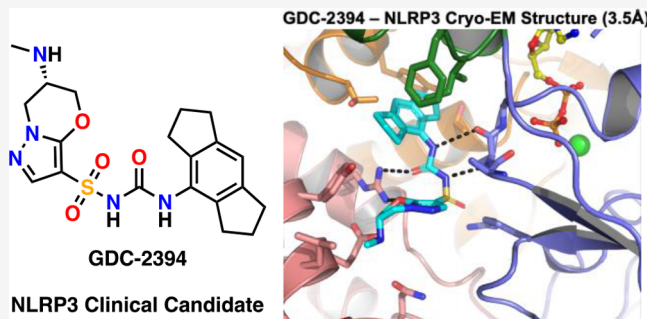
ACCESS |

Metrics & More

Article Recommendations

Supporting Information

**ABSTRACT:** Inappropriate activation of the NLRP3 inflammasome has been implicated in multiple inflammatory and autoimmune diseases. Herein, we aimed to develop novel NLRP3 inhibitors that could minimize the risk of drug-induced liver injury. Lipophilic ligand efficiency was used as a guiding metric to identify a series of 6,7-dihydro-5*H*-pyrazolo[5,1-*b*][1,3]-oxazinesulfonylureas. A leading compound from this series was advanced into safety studies in cynomolgus monkeys, and renal toxicity, due to compound precipitation, was observed. To overcome this obstacle, we focused on improving the solubility of our compounds, specifically by introducing basic amine substituents into the scaffold. This led to the identification of GDC-2394, a potent and selective NLRP3 inhibitor, with an in vitro and in vivo safety profile suitable for advancement into human clinical trials.



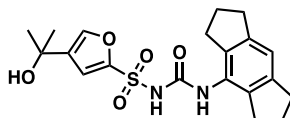
## INTRODUCTION

The maturation and release of the proinflammatory cytokines IL-1 $\beta$  and IL-18 are regulated by a group of cytosolic multiprotein complexes termed inflammasomes.<sup>1</sup> Members of the NOD-like family of receptors (NLRs) act as important cellular sensors, where NLRP3 is involved in sensing the integrity of the cytoplasm and self-assembles in response to sterile injury, or alternatively can be activated through the recognition of bacterial and other viral pathogen-associated molecular patterns in the case of NLRC4 and NLRP1.<sup>2,3</sup> Non-NLR proteins, such as Pyrin, AIM2, and CARD8,<sup>3</sup> also form inflammasomes.<sup>2</sup> Once activated, both adapter proteins and pro-caspase-1 are recruited to form distinct inflammasome complexes. Autocatalytic activation of pro-caspase-1 within the inflammasome complex results in the cleavage of pro-IL-1 $\beta$  and pro-IL-18 into their mature, active forms thereby initiating an inflammatory response. Active caspase-1 also cleaves Gasdermin D, which leads to the formation of membrane pores and initiates a form of inflammatory cell death termed pyroptosis.<sup>4</sup>

Since its reported discovery in 2004,<sup>5</sup> the NLRP3 inflammasome has been extensively investigated and identified as a key mediator of inflammation associated with sterile proinflammatory signals in a wide variety of acute and chronic human diseases such as cryopyrin-associated periodic syndromes, gout, Alzheimer's, atherosclerosis, type 2 diabetes, nonalcoholic steatohepatitis, cardiovascular disease, and numerous others.<sup>5–10</sup> Blocking activation of this pathway can potentially provide a broad therapeutic approach toward treating these inflammatory diseases.

MCC950/CRID3/CP-456773 (1), shown in Figure 1, was developed by Pfizer and first disclosed in 1998.<sup>11</sup> It was identified from a phenotypic screen of compounds that

Received: August 2, 2022

**Figure 1.** NLRP3 inhibitor MCC950/CRID3/CP-456773 (1).

suppressed IL-1 $\beta$  release in stimulated monocytes.<sup>11,12</sup> Recently, this phenotype was shown to be mediated through inhibition of inflammasome assembly, where compound 1 binds directly to the NACHT domain of NLRP3, stabilizing an inactive conformation.<sup>13–19</sup>

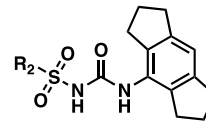
## ■ RESULTS AND DISCUSSION

**SAR and Lead Optimization.** Compound 1 was advanced into a Phase 2 clinical study as a possible treatment for rheumatoid arthritis. During this study, elevated transaminases were detected in a limited number of patients at high doses (1200 mg total daily dose, >100  $\mu$ M plasma  $C_{max}$ ), which impeded further clinical development of this compound.<sup>20</sup> While a specific cause for the off-target liver findings was never disclosed, drugs with a high total daily dose ( $\geq$ 100 mg/day) and high lipophilicity ( $\text{Log}P \geq 3$ ) typically have an increased risk for causing a drug-induced liver injury (DILI).<sup>21</sup> Given the absence of information on the off-target hepatotoxicity that was observed with compound 1, we aimed to develop a clinical candidate with reduced lipophilicity and improved potency in an effort to reduce the total dose.

Lipophilic ligand efficiency (LLE) has proven to be a useful metric in lead optimization campaigns as it enables one to evaluate the quality of a compound on both potency and lipophilicity metrics.<sup>22</sup> With compound 1 serving as a starting point for our program, we used an LLE-guided approach to identify novel and structurally diverse NLRP3 inhibitors. Additionally, we sought to identify structural replacements for the furan moiety as furans are often recognized as toxicophores that have been associated with incidences of DILI.<sup>23,24</sup>

With these goals in mind, we commenced our ligand-based drug design campaign by generating a number of aryl and heteroaryl replacements for the furan ring. A representative set of compounds are shown in Table 1. Measurement of NLRP3 activity was assessed by quantifying IL-1 $\beta$  release from LPS + nigericin stimulated human peripheral blood mononuclear cells (hPBMCs, Table 1). As a counter screen, TNF $\alpha$  levels were also measured to rule out inhibition of the TLR4/NF- $\kappa$ B signaling pathway which is required to prime the NLRP3 inflammasome prior to activation of assembly. Additionally, cell viability was monitored via the CellTiter-Glo assay to further support that decreases in IL-1 $\beta$  are not due to general cellular toxicity but due to inhibition of pyroptosis. TNF $\alpha$  production and cell viability were unaffected when compared to vehicle-treated cells (see the Supporting Information).<sup>27</sup>

Unsubstituted furan 2, which was 15-fold less potent than compound 1, served as a key benchmark to gauge our LLE-guided structural replacements in this region. Replacement of the furan with a phenyl group (3) resulted in a loss of activity and LLE. Incremental improvements in LLE could be obtained by inserting nitrogen atoms into the aromatic ring (4–7). Furan replacement with thiazole (8 and 9) could be accommodated; however, these heterocyclic replacements failed to improve potency and LLE. A loss of activity was observed with other substituted heterocycles, such as dimethyl imidazole 10 and N-methyl pyrazole 11. This decrease in

**Table 1. Furan Replacement SAR**

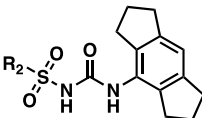
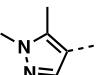
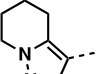
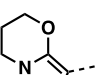
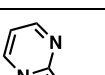
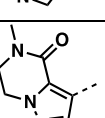
Compound	R <sub>2</sub>	IL-1 $\beta$ IC <sub>50</sub> ( $\mu$ M) <sup>c</sup>	cLogP cLogD	LLE <sup>b</sup>
1		0.029 $\pm$ 0.015 (n=50)	2.9 0.5	7.0
2		0.44	2.6 0.7	5.7
3		1.79	3.3 1.2	4.5
4		1.33	2.7 0.5	5.4
5		1.08	2.2 0.3	5.7
6		1.54	2.1 0.4	5.4
7		0.96	1.6 0.1	5.9
8		3.66	2.6 0.6	4.8
9		0.43	2.8 0.7	5.7
10		2.31	2.1 0	5.6
11		2.55	2.4 0.4	5.2
12		0.34	2.1 0.3	6.2
13		0.21	1.8 0.4	6.3

<sup>a</sup>Inhibition of the NLRP3 inflammasome pathway was assessed by quantifying IL-1 $\beta$  release from lipopolysaccharide (LPS) + nigericin stimulated hPBMCs ( $n = 1$  for all compounds except compound 1 which is reported as the geometric mean  $\pm$  SD). <sup>b</sup>LLE was calculated using the following equation: LLE = pIC<sub>50</sub> IL-1 $\beta$  – cLogD.<sup>25,26</sup>

potency was also observed in a number of *ortho* substituted phenyl analogues (i.e., Me, OMe, CN – data not shown).<sup>27</sup> Ultimately, we found that the N-methyl pyrazole regiosomers (12 and 13) proved to be adequate replacements for the furan, both exceeding the benchmark potency and LLE of unsubstituted furan 2.

With this preliminary set of furan replacements in hand, we decided to utilize N-methyl pyrazole 13 to further our SAR explorations (Table 2). Larger lipophilic N-substituted pyrazoles showed an improvement in potency (14) over smaller substituents (13). However, these substitutions were accompanied by an undesirable decrease in LLE. Consistent with our previous observations, substitution adjacent to the

**Table 2. Functionalized Pyrazole SAR**

Compound	R <sub>2</sub>	IL-1 $\beta$ IC <sub>50</sub> ( $\mu$ M) <sup>a</sup>	cLogP cLogD	LLE <sup>b</sup>
14		0.086	2.6 0.9	6.2
15		2.57	2.4 0.5	5.1
16		0.41	3.0 0.9	5.5
17		0.063 ± 0.042 (n=28)	2.0 0.4	6.7
18		0.43	2.1 0.4	6.0
19		6.2	1.8 0	5.2

<sup>a</sup>Inhibition of the NLRP3 inflammasome pathway was assessed by quantifying IL-1 $\beta$  release from LPS + nigericin stimulated hPBMCs ( $n = 1$  for all compounds except compound 17 which is reported as geometric mean  $\pm$  SD). <sup>b</sup>LLE was calculated using the following equation: LLE = pIC<sub>50</sub> IL-1 $\beta$  - cLogD.

aryl-S connection were detrimental to potency (15); however, we discovered that the potency could be restored by cyclizing the two pyrazole substituents to form the fused bicyclic pyrazole 16. We were encouraged to see that further improvements to potency and LLE could be made by introducing an oxygen atom into the saturated fused ring system to generate the 3-substituted-6,7-dihydro-5H-pyrazolo-[5,1-*b*][1,3]oxazine (17). Other fused bicyclic systems were also investigated, specifically to explore the potential H-bond accepting nature of the oxygen in the oxazine ring (e.g., 18 and 19); however, these compounds failed to eclipse the efficiency profile of compound 17. Having identified a compound that accomplished one of our main goals (i.e., to identify a structural replacement to the furan), we decided to progress 17 into a series of in vitro and in vivo studies to de-risk any potential safety liabilities (Figure 2).

The potency of 17 was further evaluated in a whole blood (WB) assay which measures NLRP3 activity by quantifying IL-1 $\beta$  release from LPS + ATP stimulated human WB. The IC<sub>50</sub>/IC<sub>90</sub> values for 17 were  $1.21 \pm 1.34 \mu\text{M}$  and  $6.49 \pm 6.48 \mu\text{M}$  ( $n = 102$ ), respectively, which were on par with the human WB IC<sub>50</sub>/IC<sub>90</sub> values for compound 1 (IC<sub>50</sub> =  $1.58 \pm 1.27 \mu\text{M}$ ; IC<sub>90</sub> =  $7.24 \pm 5.13 \mu\text{M}$  ( $n = 136$ )). The right shift in potency that is observed between the PBMC and WB assays can directly be attributed to the relatively high levels of plasma

protein binding, resulting in a relatively low free fraction of drug.

Compound 17 had moderate kinetic solubility ( $102 \mu\text{M}$  in 1X PBS buffer pH 7.4) and moderate permeability in gMDCK<sup>28</sup> and was stable in hepatocytes across species. The pharmacokinetic profiles of 17 across species were relatively similar to one another and generally correlated well with our in vitro data. Compound 17 typically had low-moderate levels of oral bioavailability (%F), low clearance, and small volumes of distribution (Figure 2B).

Compound 17 was profiled in several in vitro safety assays, such as hERG, BSEP, cytotoxicity, and GSH trapping (Figure 2A). No significant safety signals were identified in these assays prompting us to progress it into in vivo safety studies.

Upon testing 17 in vivo, renal toxicity was identified in the cynomolgus monkey after oral dosing at  $\geq 100 \text{ mg/kg/day}$  ( $\geq 282 \text{ h } \mu\text{g/mL}$ ) for 14 days. Specifically, increased kidney weights, elevated blood urea nitrogen (BUN) levels, retrograde nephropathy, and ghost crystals were noted in male and/or female animals (Figure 2C).

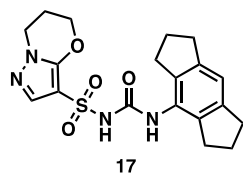
Retrograde nephropathy, due to compound precipitation (as parent or metabolite), and the presence of crystals in the kidney (ghost crystals) have been linked to several key pharmacokinetic properties that include solubility, dose, route of elimination, and metabolite profiles.<sup>24</sup> Ultimately, upon further analysis we were able to determine that the crystalline precipitates were parent drugs.

The pH of the fluid in the kidney of cynomolgus monkeys typically ranges from 6.4 to 8.2.<sup>29</sup> We suspected that precipitation of compound 17 could be occurring at lower pH values because this type of solubility profile would be consistent with what would be expected for a sulfonylurea ( $pK_a \sim 5$ ). As a result, we determined the solubility of 17 at various pH values and confirmed that it precipitously decreases at lower pH (Figure 3). We believed that this solubility phenomenon was the most probable cause for the observed renal toxicity.

With this information in hand, we rationalized that the most straightforward way to improve the solubility of our sulfonylurea-based series of NLRP3 inhibitors would be to introduce a basic substituent into the scaffold. The prospect of shifting our designs toward a zwitterionic chemical space presented the team with additional opportunities to further improve upon the quality and efficiency of our existing leads as zwitterionic compounds typically have improved solubility profiles and larger volumes of distribution and exhibit lower binding to plasma proteins, compared to acidic compounds.

After a brief SAR investigation (not shown), we were able to determine that the 6-position (R<sub>3</sub>) of the oxazine ring was able to accommodate a wide array of substitution patterns and functional groups (e.g., OMe, Me, *gem*-dimethyl). Focusing specifically on the introduction of various basic amine substituents (Table 3), installation of an amino methyl group (20) improved potency by >10-fold and LLE by 1.5 units compared to the unsubstituted scaffold (17). There was a strong stereochemical preference as 20 was >250-fold more potent than its enantiomer R-20. The absolute stereochemical assignment of compound 20 was determined based on the known chirality of starting material ((S)-methyl 2-((tert-butoxycarbonyl)amino)-3-hydroxypropanoate) that was utilized in the synthesis.

Other amines, such as such dimethylamine (21) and 3-methoxy-azetidine (22), were also tolerated and showed



(A)

In vitro Candidate Profile of 17	
PBMC IL-1 $\beta$ IC <sub>50</sub> ( $\mu$ M) <sup>a</sup>	0.063 ± 0.042 (n = 28)
WB IC <sub>50</sub> / IC <sub>90</sub> ( $\mu$ M) <sup>b</sup>	1.21 ± 1.34 / 6.49 ± 6.48 (n = 102)
CL <sub>Heps</sub> H / R / M / D / C (mL/min/kg)	< 6.2 / < 10 / < 21 / < 7.9 / < 8.8
gMDCK Papp (A:B) ( $10^{-6}$ cm × s <sup>-1</sup> )	1.8
kinetic solubility ( $\mu$ M)	102
PPB H / R / M / D / C (%)	98.6 / 98.6 / 99.1 / 95.5 / 96
Cytotoxicity-Primary Hepatocytes ( $\mu$ M)	>100
Cytotoxicity-3D InSphero ( $\mu$ M)	>100
BSEP IC <sub>50</sub> ( $\mu$ M)	>100
GSH Trapping	Negative
hERG 2pt 1 $\mu$ M / 10 $\mu$ M (% inh)	4.1 / 9.7

(B)

Preclinical PK				
Species	Mouse	Rat	Dog	Cyno
CL <sub>p</sub> (mL/min/kg)	1.3	2.4	1.0	1.3
V <sub>ss</sub> (L <sup>*</sup> Kg <sup>-1</sup> )	0.2	0.2	0.2	0.08
T <sub>1/2 (IV)</sub> (h)	1.9	1.1	2.9	1.4
%F (1 mg × kg <sup>-1</sup> )	18	30	28	17

(a) Reported as geometric mean ± SD (b) Assay performed with human whole blood in triplicate with LPS priming and test compounds for 3 hours followed by ATP activation for 1 hour then measurement of IL-1 $\beta$  in plasma; reported as geometric mean ± SD

(C)

Summary of Renal Findings of 17			
Dose (mg/kg)	Gross Observations	Clinical Chemistry	Histopathology
30	Increased kidney weights (M)	None	None
100	Increased kidney weights (M&F)	Elevated BUN levels (F)	Retrograde nephropathy (F) Evidence of ghost crystals
300	Increased kidney weights (M&F)	Elevated BUN levels (F)	Retrograde nephropathy (M&F) Evidence of ghost crystals

**Figure 2.** (A) In vitro candidate profile of 17. (B) Cross species PK profiles of 17. (C) Summary of renal toxicities observed in a 14-day dose range finding study in cynomolgus monkeys.

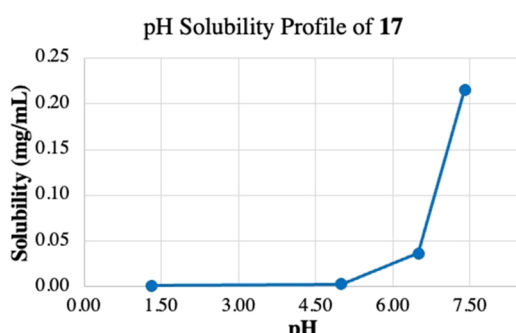


**Figure 3.** Solubility profile of 17.

improvements in both potency and LLE compared to 17. While encouraging, these iterative designs had moderate human liver microsome stability and failed to improve upon the ligand efficiency of 20. Homologation of the dimethyl amino group (23) was also explored; however, this modification was detrimental to potency.

Encouraged by these results, we decided to profile compound 20 as a potential candidate. In comparison to our previous lead (17), 20 displayed a differential pH-dependent solubility profile (Figure 4). Importantly, a dramatic increase in solubility was observed at lower pH values. Additionally, the human WB potency was improved by 3-fold; this improvement in potency can be attributed, in part, due to the reduced PPB (Figure 5A). Compound 20 generally had good in vitro—in vivo correlation, exhibiting low-moderate clearance across species. Despite the poor measured permeability in the

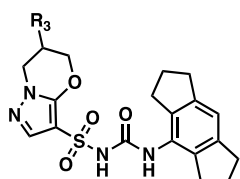
gMDCK assay, moderate-high levels of oral exposure were observed. Shifting to the zwitterionic scaffold had a minor impact on increasing the volume of distribution ( $V_{ss}$ ). Furthermore, compound 20 was clean in our in vitro safety assessment, which further supported our decision to progress it into in vivo safety studies.

Cynomolgus monkeys were dosed up to 500 mg/kg/day (1210 h.  $\mu$ g/mL) for 14 days, and no kidney or liver-related findings were identified. There were no test-article related findings in serum chemistry, hematology, urinalysis, or urine chemistry, and only minimal thymic lymphoid depletion was noted at doses  $\geq$ 300 mg/kg (1050 h  $\mu$ g/mL) in the histopathology examination.

## ■ IN VITRO CHARACTERIZATION OF GDC-2394 (20)

**Inflammasome Selectivity for GDC-2394 (20).** To determine inflammasome selectivity, we performed assays to assess caspase-1 activation in THP 1 cells after NLRP3 or NLRC4 inflammasome activation using LPS plus nigericin (to activate NLRP3) or flagellin (to activate NLRC4). Compound 20 inhibited NLRP3-induced caspase-1 activity in a concentration-dependent manner but did not inhibit NLRC4-dependent inflammasome activation. The mean IC<sub>50</sub> of compound 20 was determined to be  $0.051 \mu$ M ± 0.033 (n = 4) for NLRP3-dependent caspase-1 activation in THP1 cells (Figure 6A) and  $0.063 \pm 0.006 \mu$ M (n = 2) for NLRP3-dependent IL-1 $\beta$  release from mouse bone marrow-derived macrophages (BMDMs) (Figure 6C) and  $>20 \mu$ M for NLRC4-dependent inflammasome activation in both human and mouse cells (Figure 6B,D).

**Table 3.** 6,7-Dihydro-5H-pyrazolo[5,1-*b*][1,3]oxazine Substitutions



Compound	R <sub>3</sub>	IL-1 $\beta$ IC <sub>50</sub> ( $\mu$ M) <sup>c</sup>	cLogP cLogD	LLE <sup>d</sup>
GDC-2394 (20)	H N	0.0054 ± 0.004 (n=16)	1.1 0.1	8.2
<i>R</i> -20	H N	1.40	1.1 0.1	5.8
21 <sup>a</sup>	I N	0.013 ± 0.008 (n=3)	1.6 0.4	7.5
22 <sup>a</sup>	MeO N	0.012 ± 0.01 (n=3)	1.2 0.1	7.8
23 <sup>b</sup>	N I	2.40	1.7 -0.1	5.7

<sup>a</sup>Data reported for the most potent stereoisomer. <sup>b</sup>Tested as the racemate. <sup>c</sup>Inhibition of the NLRP3 inflammasome pathway was assessed by quantifying IL-1 $\beta$  release from LPS + nigericin stimulated hPBMCs (reported as geometric mean ± SD; compounds *R*-20 and 23 are reported as *n* = 1). <sup>d</sup>LLE was calculated using the following equation: LLE = pIC<sub>50</sub> IL-1 $\beta$  - cLogD.

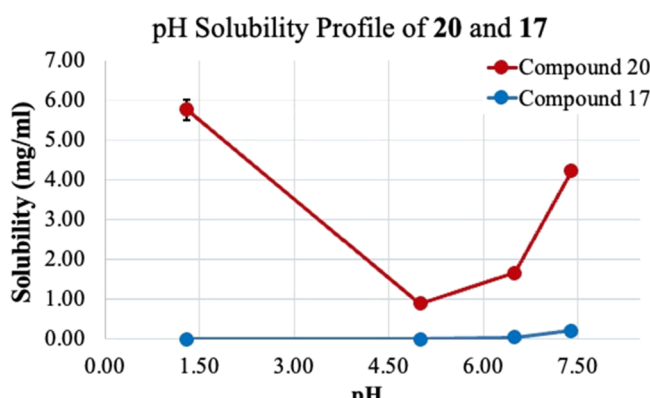


**Figure 4.** Solubility profiles of 20 and 17.

**GDC-2394 (20) Inhibits NLRP3-Induced Apoptosis Associated Speck-Like Protein Containing CARD (ASC) Speck Formation in THP-1 Cells.** NLRP3 inflammasome activation requires ASC for the activation of caspase-1. After inflammasome activation, ASC assembles into large protein complex, termed “specks”. ASC specks can be observed as they reach a size of approximately 1  $\mu$ m and, in most cells, only one speck forms upon inflammasome activation. We utilized a human monocytic THP-1 cell line (Invivogen) that stably expresses a 37.6 kDa ASC:GFP fusion protein to monitor speck formation by microscopy after activation of the NLRP3-dependent inflammasome pathway (Figure 7A,B). Compound 20 inhibited LPS plus nigericin-induced ASC speck formation

in THP-1 cells in a concentration-dependent manner, with an IC<sub>50</sub> of 0.048  $\mu$ M (Figure 7).

**GDC-2394 (20) Inhibits Production of IL-1 $\beta$  in Human and Mouse WB after Activation of the NLRP3 Inflammasome with LPS and ATP.** To assess the ability of GDC-2394 (20) to inhibit IL-1 $\beta$  production in both human and mouse WB, we performed activation assays with ATP together with priming by LPS using blood from multiple donors. We observed that compound 20 was able to inhibit IL-1 $\beta$  levels with similar potency across the two species (Table 4).

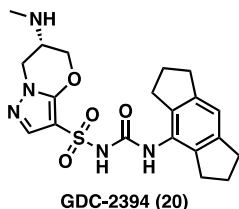
**GDC-2394 (20) Inhibits Production of IL-1 $\beta$  in Human WB after Crystal Activation of the NLRP3 Inflammasome.** To assess the ability of compound 20 to inhibit production of IL-1 $\beta$  after activation by crystals previously described to activate the NLRP3 inflammasome, we stimulated LPS-primed human blood with monosodium urate (MSU) crystals, calcium pyrophosphate dehydrate (CPPD), or cholesterol crystals followed by the measurement of IL-1 $\beta$  in isolated plasma. We observed concentration-dependent inhibition of IL-1 $\beta$  levels in the blood plasma with compound 20 (Figure 8).

**GDC-2394 (20) Inhibits Human Macrophage IL-1 $\beta$  and IL-18 Production after Activation of the NLRP3 Inflammasome.** To assess the ability of compound 20 to inhibit production of IL-1 $\beta$  and IL-18 after activation of NLRP3 in macrophages, we stimulated human monocyte-derived macrophages with either LPS plus ATP or LPS plus cholesterol crystals followed by measurement of IL-1 $\beta$  and IL-18 levels in the culture supernatants. We observed concentration-dependent inhibition of IL-1 $\beta$  and IL-18 production in stimulated human monocyte-derived macrophages with compound 20 (Figure 9).

## CRYO-EM STRUCTURE OF NLRP3 WITH GDC-2394 (20)

Intrigued by the SAR on the pyrazolo-oxazine ring and encouraged by recent advances in NLRP3 structural biology,<sup>17,19,30–32</sup> we sought to obtain a structural understanding of how compound 20 binds to NLRP3. Using a construct representing residues K131-W1036 of NLRP3 fused to NEK7 (NLRP3 complex), 20 was added to the NLRP3 complex prior to EM grid preparation and data collection. We developed a cryo-EM data processing and refinement workflow,<sup>33</sup> resulting in a 3.5  $\text{\AA}$  resolution map that allowed us to unambiguously build compound 20 into the Coulomb potential map. The structure reveals that compound 20 binds to an allosteric pocket in the NACHT domain with the binding site at the interface of the NBD, HD1, WHD, and HD2 subdomains, and residues from each of these subdomains interact with the compound (Figure 10).

The hexahydro-s-indacene moiety sits in a cavity which is largely hydrophobic in nature and sandwiched by F410 and I411 sidechains above and T439 and Y443 sidechains below the plane of the rings. The urea extends into a channel between the NBD and the HD2 domains interacting with the mainchain atoms of A228 of the Walker A motif and the sidechain of R578 from HD2. The sidechains of R351 and R578 create a basic pocket surrounding the sulfonamide oxygen atoms. The pyrazole ring lies across the opening of the allosteric pocket that is connected to the bulk solvent but does not appear to engage in any direct interactions with the protein. In contrast, the oxygen of the substituted oxazine is within a H-bond distance of the R578 sidechain and with the saturated ring and



(A) GDC-2394 (20)

(B)

In vitro Candidate Profile of GDC-2394 (20)	
PBMC IL-1 $\beta$ IC <sub>50</sub> ( $\mu$ M) <sup>a</sup>	0.0054 ± 0.004 (n=16)
WB IC <sub>50</sub> / IC <sub>90</sub> ( $\mu$ M) <sup>b</sup>	0.40 ± 0.43 / 1.47 ± 1.52 (n = 152)
CL <sub>HepG</sub> H / R / M / D / C (mL/min/kg)	< 6.2 / < 10 / < 21 / < 7.9 / < 8.8
gMDCK Papp (A:B) ( $10^{-6}$ cm × s <sup>-1</sup> )	0.077
kinetic solubility ( $\mu$ M)	105
PPB H / R / M / D / C (%)	95.6 / 93 / 97.6 / 88.6 / 91.8
Cytotoxicity-Primary Hepatocytes ( $\mu$ M)	>100
Cytotoxicity-3D InSphero ( $\mu$ M)	>100
BSEP IC <sub>50</sub> ( $\mu$ M)	>100
GSH Trapping	Negative
hERG 2pt 1 $\mu$ M / 10 $\mu$ M (% inh)	-3.1 / 0.2

(a) Reported as geometric mean ± SD (b) Assay performed with human whole blood in triplicate with LPS priming and test compounds for 3 hours followed by ATP activation for 1 hour then measurement of IL-1 $\beta$  in plasma; Reported as geometric mean ± SD

Figure 5. (A) In vitro candidate profile of GDC-2394 (20). (B) Cross species PK profiles of GDC-2394 (20).

Preclinical PK				
Species	Mouse	Rat	Dog	Cyno
CL <sub>p</sub> (mL/min/kg)	10.1	1.3	11.7	4.1
Vss (L*Kg <sup>-1</sup> )	0.72	0.29	0.67	0.18
T <sub>1/2 (IV)</sub> (h)	1.2	4.4	0.99	0.89
%F (1 mg × kg <sup>-1</sup> )	80	33	78	53

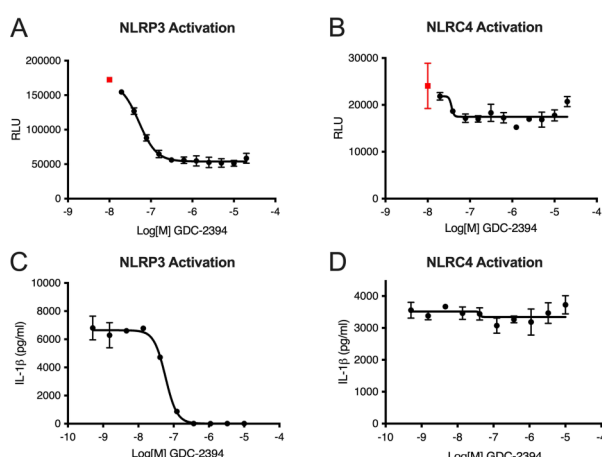


**Figure 6.** Selectivity of compound 20 in human and mouse cells. (A) NLRP3-dependent caspase-1 activation of compound 20 in THP-1 cells. (B) NLRC4-dependent inflammasome activation of compound 20 in THP-1 cells; data are the representation of four independent experiments. (C) NLRP3-dependent IL-1 $\beta$  release in mBMDMs. (D) NLRC4-dependent IL-1 $\beta$  release in mBMDMs; data are the representation of two independent experiments. Red points indicate the vehicle controls in the caspase-1 assays.

methylamine packing up against sidechains of L628 and E629 from HD2, thus providing a rationale for the improved potency observed from these substituents.

## ■ IN VIVO ASSESSMENT OF GDC-2394

**GDC 2394 (20) Inhibits In Vivo Production of IL-1 $\beta$  in an Acute Mouse Peritonitis Model.** The in vivo potency of orally delivered compound 20 in blocking NLRP3 activation was evaluated in an acute mouse peritonitis model using intraperitoneal administration of LPS and MSU. Compound 20 treatment resulted in a dose-dependent decrease in peritoneal IL-1 $\beta$  concentrations after MSU administration, and compared with the control, the level of IL-1 $\beta$  was decreased by 66.8 and 81.3% ( $p < 0.001$ ) at 1 and 10 mg/kg of

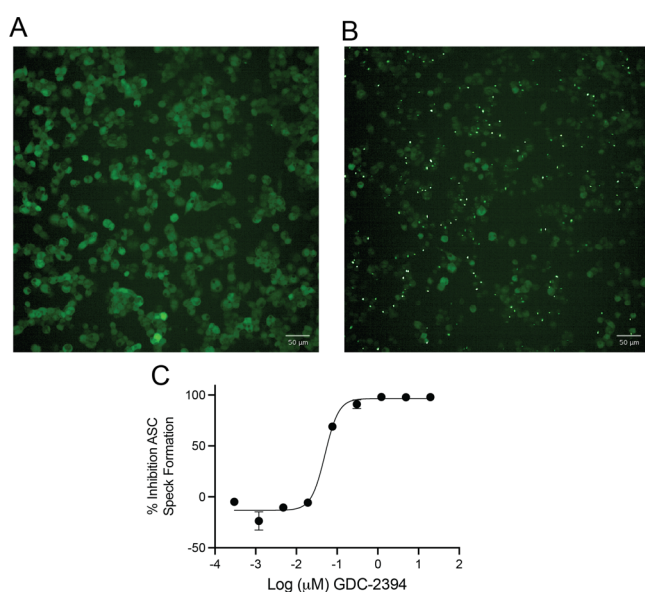


**Figure 7.** Inhibition of ASC speck formation by compound 20. THP-1 ASC-green fluorescent protein (GFP) cells were used to monitor speck formation by microscopy. (A) Presence of cytoplasmic ASC-GFP expression after priming with LPS. (B) Formation of macromolecular, micrometer-sized ASC-GFP complexes after additional treatment with nigericin. (C) Concentration-dependent inhibition of ACS-GFP speck formation by compound 20 ( $IC_{50} = 0.048 \mu$ M ( $n = 32$ )). 50  $\mu$ m scale is indicated in each image; pictures were taken with a 20 $\times$  objective. Data are plotted as means and standard deviation of three replicates.

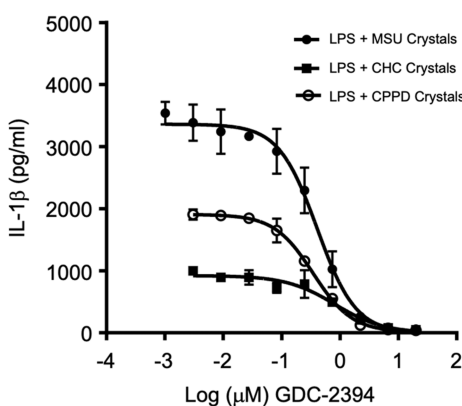
compound 20, respectively (Figure 11A). Satellite PK analysis indicated that the oral exposures with 1 mg/kg and 10 mg/kg compound 20 covered the mouse whole blood (MWB) IL-1 $\beta$  IC<sub>90</sub> value (0.39  $\mu$ M) for ~4 and ~14 h, respectively (Figure 11B).

**GDC 2394 (20) Reduces Paw Swelling and Pain in a Functional Rat Model of Gouty Arthritis.** Compound 20

**Table 4. Inhibition of IL-1 $\beta$  by GDC-2394 (20) Following NLRP3 Activation with LPS plus ATP in Human and Mouse WB<sup>a</sup>**

species	IC <sub>50</sub> ± SD (μM)	IC <sub>70</sub> ± SD (μM)	IC <sub>90</sub> ± SD (μM)	n
human	0.40 ± 0.43	0.66 ± 0.63	1.47 ± 1.52	152
mouse	0.10 ± 0.02	0.18 ± 0.03	0.39 ± 0.07	10

<sup>a</sup>Reported as geometric means of the indicated number (n) of blood donors.

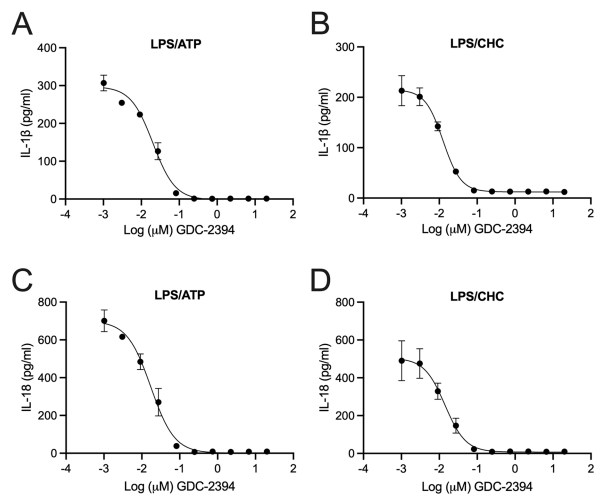


Stimulation	Reduction in IL-1 $\beta$ Levels		
	IC <sub>50</sub> ± SD (μM)	IC <sub>70</sub> ± SD (μM)	IC <sub>90</sub> ± SD (μM)
LPS + MSU	0.38 ± 0.05	0.69 ± 0.11	1.76 ± 0.41
LPS + CHC	0.49 ± 0.25	0.94 ± 0.68	2.61 ± 3.02
LPS + CPPD	0.29 ± 0.07	0.59 ± 0.11	1.81 ± 0.22

**Figure 8.** Inhibition of IL-1 $\beta$  by compound 20 following NLRP3 activation with LPS plus crystal stimulation in human WB. Data are plotted as means and standard deviation. LPS = lipopolysaccharide; MSU = monosodium urate; CHC = cholesterol crystals; CPPD = calcium pyrophosphate dihydrate. SD = standard deviation. IC<sub>50</sub> = 50% inhibitory concentration; IC<sub>70</sub> = 70% inhibitory concentration; IC<sub>90</sub> = 90% inhibitory concentration reported as geometric means of three donors.

(which had an oral exposure that covered the IL-1 $\beta$  IC<sub>90</sub> in MWB<sup>34</sup> for at least 14 h with a single dose of 10 mg/kg) was tested in a rat model of gouty arthritis that incorporated an intra-articular injection of MSU crystals to stimulate joint inflammation. Anakinra (IL-1 $\beta$  receptor antagonist) and colchicine (microtubule inhibitor) were also tested as positive controls relevant to the current clinical standard of care. Knee swelling was significantly inhibited by compound 20 after 48 h ( $p < 0.001$ ), and this inhibition continued for 6 days (Figure 12A). Similar magnitudes of inhibition were observed for anakinra and colchicine. With respect to pain, the threshold for mechanical allodynia was significantly inhibited by compound 20 by 48 h ( $p < 0.001$ ) (Figure 12B), and the level of inhibition was also comparable to anakinra and colchicine. The inhibitory effects of compound 20 persisted through day 6 of the study.

**Human Dose Prediction.** While the *in vivo* PKPD model confirmed that there was a dose-dependent response on activity, we believe that the human whole blood (HWB) assay is the most clinically translatable data for estimating human



	IC <sub>50</sub> ± SD (μM)	IC <sub>70</sub> ± SD (μM)	IC <sub>90</sub> ± SD (μM)
<b>IL-1<math>\beta</math></b>			
LPS + ATP	0.016 ± 0.007	0.03 ± 0.016	0.079 ± 0.056
LPS + CHC	0.017 ± 0.006	0.03 ± 0.016	0.068 ± 0.066
<b>IL-18</b>			
LPS + ATP	0.017 ± 0.013	0.03 ± 0.024	0.074 ± 0.063
LPS + CHC	0.017 ± 0.013	0.03 ± 0.028	0.072 ± 0.089

**Figure 9.** Inhibition of IL-1 $\beta$  and IL-18 by compound 20 following NLRP3 activation with LPS plus ATP (A,C), or LPS plus cholesterol stimulation (B,D), in human monocyte-derived macrophages. Data are plotted as means and standard deviation. Table data represent IC<sub>50</sub>, IC<sub>70</sub>, and IC<sub>90</sub> geometric means from four donors.

dose (Table 5). As a result, prediction of human clearance (CL) and volume of distribution ( $V_{ss}$ ) for compounds 1, 17, and 20 was performed by allometric scaling on the basis of the eq CL =  $aW^b$ , where  $a$ ,  $W$ , and  $b$  are the allometric coefficient, body weight, and allometric exponent, respectively.<sup>35–37</sup> Total CL and  $V_{ss}$  values obtained from PK studies in preclinical species were scaled on the basis of body weight to predict the systemic CL and  $V_{ss}$  in humans. Body weights of 0.02, 0.25, 8, 4, and 70 kg were used for mice, rats, dogs, monkeys, and humans, respectively. The predicted efficacious dose in human covering HWB (LPS + 1.75 mM ATP) IC<sub>50</sub> and IC<sub>90</sub> as trough concentrations for 24 h was simulated using a one-compartment model and a bioavailability predicted from the bioavailability observed in preclinical species.

## ■ CHEMISTRY

**Synthesis of Compound 17.** 1,2-Dihydro-pyrazole-3-one was heated with 1,3-dibromopropane potassium carbonate in DMF to deliver pyrazolo-oxazine 25 (Figure 13). Pyrazolo-oxazine 25 was heated with chlorosulfonic acid to generate the corresponding sulfonyl chloride, which was subsequently reacted with ammonia to give sulfonamide 26. The sodium salt of sulfonamide 26, which was generated using sodium methoxide in methanol, was added to 4-isocyanato-1,2,3,5,6,7-hexahydro-s-indacene to deliver the desired product, sulfonylurea 17, in 17% overall yield.

**Synthesis of GDC-2394 (20).** (S)-Methyl 2-((tert-butoxycarbonyl)amino)-3-hydroxypropanoate (27) was chlorinated with hexachloroethane and triphenylphosphine to yield 28 (Figure 13). The methyl ester was reduced with lithium borohydride to generate amino alcohol 29. The Mitsunobu

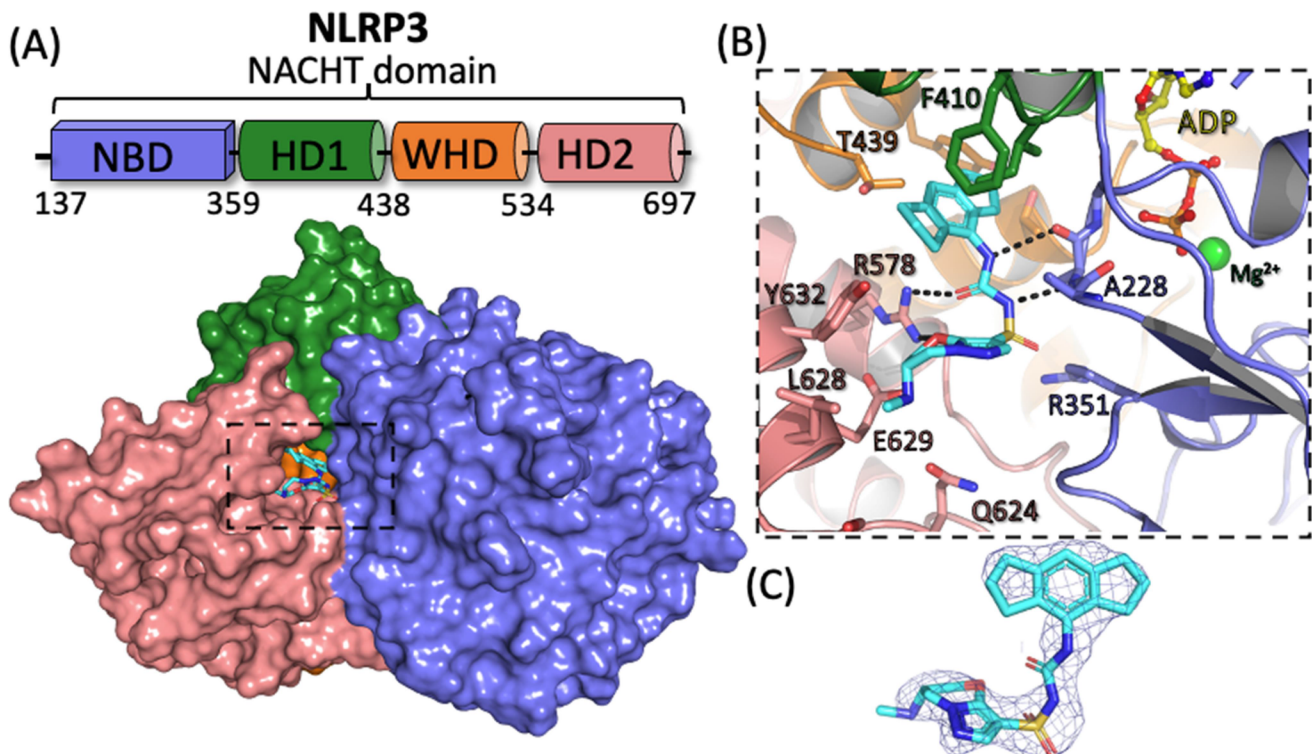


**Figure 10.** (A) Schematic and surface representation of the NACHT domain of NLRP3 colored according to the subdomains (NBD – nucleotide binding domain, HD1 = helical domain 1, WHD = winged helix domain, and HD2 = helical domain 2). The allosteric binding site of GDC-2394 (20) is highlighted by the dashed rectangle. (B) Close up view of the interactions of GDC-2394 bound to the allosteric site in the NACHT domain of NLRP3. Coloring is according to (A) with the carbon atoms of GDC-2394 colored cyan and hydrogen bond interactions depicted as dashes. (C) 3.5 Å Coulomb potential map of GDC-2394 showing that all atoms of the compound are well-defined by the map. The coordinates for the cryoEM structure of NLRP3 NACHT domain have been deposited at the RCSB with the PDB-ID 8ETR.

reaction with 1-acetyl-1,2-dihydro-3H-pyrazol-3-one gave exclusively the O-alkylated alkyl chloride **30**. A one-pot deacetylation and cyclization was accomplished by heating alkyl chloride **30** with potassium carbonate in methanol to deliver pyrazolo-oxazine **31**. Methylation of the amine was carried out with sodium hydride and methyl iodide in the presence of triethylamine to give compound **32**. The Boc-protecting group was removed with HCl in dioxane. The resulting amine was subsequently protected with TFAA to deliver trifluoroacetamide **33**. Sulfenylation of trifluoroacetamide **33** was carried out using chlorosulfonic acid followed by treatment with pyridine and then  $\text{PCl}_5$ . Ammonia was then introduced into the reaction to generate sulfonamide **34**. The sodium salt of sulfonamide **34**, which was generated using sodium hydride, was added to 4-isocyanato-1,2,3,5,6,7-hexahydro-s-indacene to form sulfonylurea **35**. Finally, the trifluoroacetamide-protecting group was removed with sodium hydroxide to deliver the desired product, GDC-2394 (**20**), in 10% overall yield.

## CONCLUSIONS

In summary, we utilized LLE as a central metric to guide our early medicinal chemistry efforts toward identifying a novel series of NLRP3 inhibitors that aimed at (1) eliminating the furan toxicophore and (2) reducing the LogP compared to the literature lead, MCC950 (**1**). These efforts lead us to identify a series of 6,7-dihydro-5H-pyrazolo[5,1-*b*][1,3]oxazine-3-sulfonylurea NLRP3 inhibitors which broadly eliminate the furan structural alert. Compounds **17** and GDC-2394 (**20**) were identified as leading compounds from our work, and both

compounds had significantly reduced lipophilicity compared to the literature lead (clogP: **1** = 2.9; **17** = 2.0; **20** = 1.1). With the elimination of the potential toxicophoric furan moiety and more efficient deployment of lipophilicity, compounds from this series have distinct advantages over previously reported NLRP3 inflammasome inhibitors.

We progressed and profiled compounds **17** and **20** into safety studies *in vivo*. Renal toxicity was observed with our initial lead (**17**) in cynomolgus monkeys, which was attributed to an inadequate compound solubility profile at pH values typically observed in cynomolgus kidneys (e.g., 6.4–8.2). As a result, we shifted our medicinal chemistry efforts toward identifying compounds with improved solubility profiles within a zwitterionic chemical space. This was accomplished by introducing a basic amine into the scaffold, which led to the identification of GDC-2394 (**20**), a compound with improved solubility and potency. The cryo-EM structure of **20** in complex with the NLRP3 complex provided a structural rationale for the potency gain from the amino methyl substituent. Compound **20** was advanced into *in vivo* safety studies in cynomolgus monkeys where no renal or hepatic test-article related findings were noted at doses up to 500 mg/kg/day for 14 days.

In line with expectations for *bona fide* NLRP3 inhibitors, compound **20** inhibited production of IL-1 $\beta$  in human and mouse WB in response to LPS priming and activation by ATP, and also LPS priming and activation by MSU crystals, calcium pyrophosphate dehydrate, and cholesterol crystals in HWB and macrophages. In an acute peritonitis model, compound **20** reduced peritoneal cavity IL-1 $\beta$  production, and in a rodent

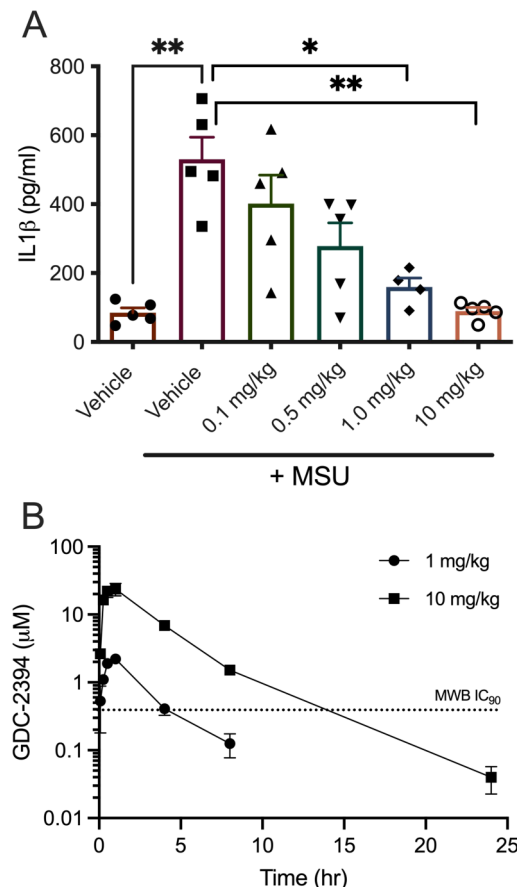


**Figure 11.** (A) Dose-dependent reduction of IL-1 $\beta$  in response to acute stimulation with LPS and MSU in the peritoneal cavity by compound 20. Mice were given an oral dose of compound 20. 2 h later, 1.25  $\mu$ g of LPS was injected IP, and then 1 mg of MSU crystals was injected IP after a further 2 h. 30 min after the MSU injection, the mice were culled, and peritoneal lavage was collected and analyzed for IL-1 $\beta$  protein levels. Error bars represent the standard error of the mean. \* $p < 0.05$ ; \*\* $p < 0.01$  using the Mann–Whitney test. (B) Mouse blood concentration of compound vs time profiles after dosing with 1 and 10 mg/kg of compound 20. Data represent mean and standard deviation of three animals per group, and MWB IC<sub>90</sub> concentration is annotated.

model of gouty arthritis induced by intra-articular injection of MSU crystals, it significantly reduced joint swelling and pain scores, comparable to that achieved by IL-1 $\beta$  blockade. Compound 20 thus behaved as expected for an NLRP3 inhibitor both in vitro and in vivo.

Preliminary human dose predictions were determined for compounds 1, 17, and GDC-2394 (20) using predicted human PK from allometric scaling and covering the HWB IC<sub>50</sub>/IC<sub>90</sub> as trough concentrations for 24 h. The dose prediction for compound 1 was 850 mg QD (covering IC<sub>50</sub>), whereas compounds 17 and 20 had predicted doses of 1200 mg QD and 500 mg QD (covering IC<sub>50</sub>) respectively. The improved HWB potency, solubility, and oral bioavailability profiles of compound 20 contributed toward lowering the predicted human dose.

## EXPERIMENTAL SECTION

**Chemistry. General Methods.** All commercial reagents and anhydrous solvents were used without additional purification. Reactions involving air and/or moisture sensitive reagents were

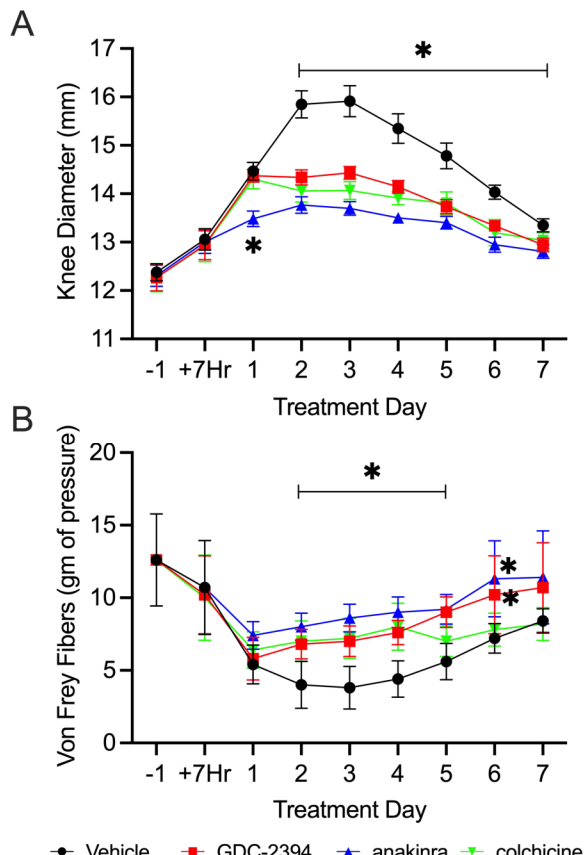
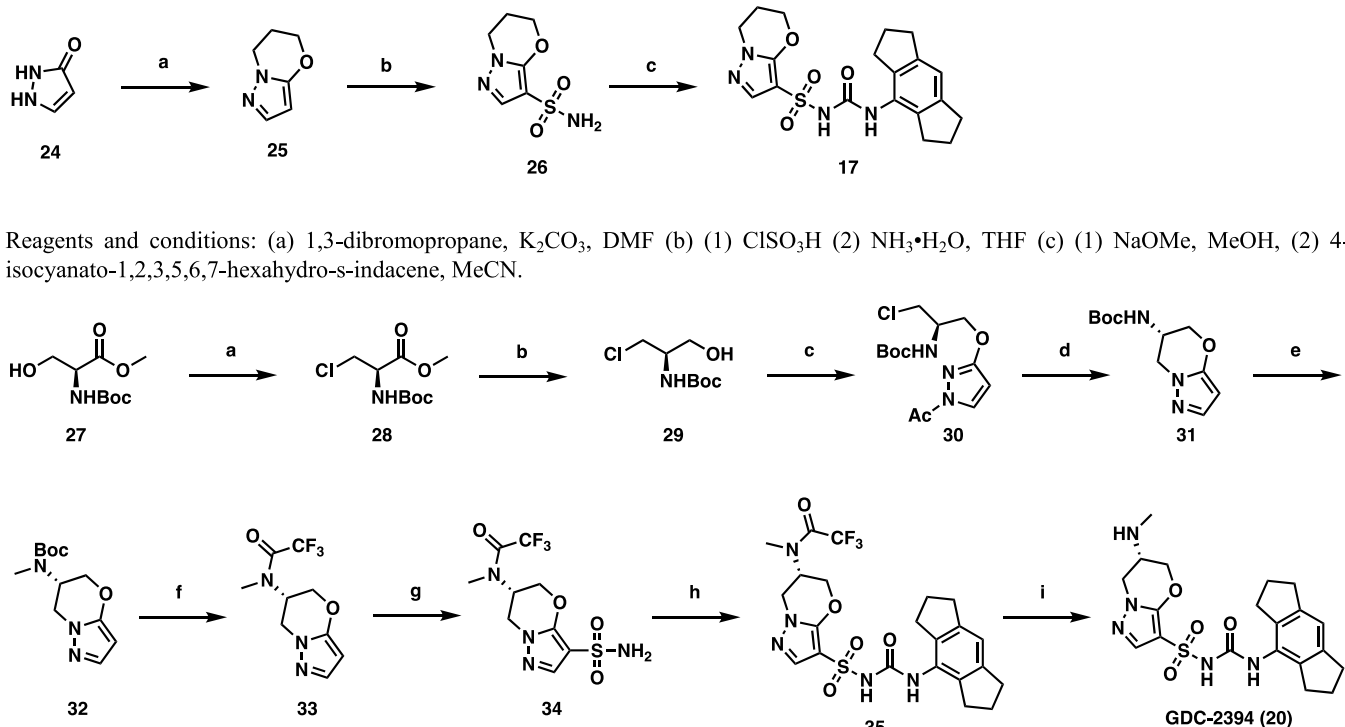


**Figure 12.** Reduction in swelling and pain by compound 20. 25 mg/kg compound 20, 50 mg/kg IL-1 receptor antagonist (anakinra, an IL-1 $\beta$  inhibitor), or 0.5 mg/kg colchicine (a microtubule inhibitor that blocks cytokine secretion) were dosed in an interventional setting in rats 3 h after the intra-articular injection and continued once daily for 7 days. The effect on the clinical endpoints of swelling (A) and pain (B) was measured daily. Data are plotted as the mean of 10 animals per group, and error bars represent the standard deviation. \* $p < 0.01$  versus the corresponding vehicle group timepoint using the t test; the bar indicates that all treatment groups met statistical significance versus the vehicle for those timepoints.

**Table 5. Human Dose Predictions for Compounds 1, 17, and GDC-2394 (20)**

compound	1	17	GDC-2394 (20)
CL (mL/min/kg)	0.8	1.1	1.5
V <sub>ss</sub> (L kg <sup>-1</sup> )	0.1	0.1	0.3
t <sub>1/2</sub> (h)	1.8	1.6	2.3
F (%)	57	25	61
QD dose covering IC <sub>50</sub> C <sub>trough</sub> (mg)	850	1200	500
QD dose covering IC <sub>90</sub> C <sub>trough</sub> (mg)	7000	9500	2400

carried out under a nitrogen atmosphere. Nuclear magnetic resonance (NMR) spectra were acquired on a Bruker BioSpin GmbG operating at 400 and 100 MHz for <sup>1</sup>H and <sup>13</sup>C, respectively, and are referenced internally according to residual solvent signals. NMR data were processed using MNova software and recorded as follows: <sup>1</sup>H NMR – chemical shift ( $\delta$ , ppm), multiplicity (s, singlet; d, doublet; t, triplet; q, quartet; p, pentet; m, multiplet), coupling constant (Hz), and integration; <sup>13</sup>C NMR – chemical shift ( $\delta$ , ppm). High-resolution mass spectra were recorded on a Thermo Scientific Orbitrap Q Exact mass spectrometer. Thin-layer chromatography was performed on EMD TLC Silica gel 60 F254 plates and visualized with UV light. Reactions were monitored using a Shimadzu LCMS/UV system with LC-30 AD solvent pump, 2020 MS, a Sil-30 AC autosampler, an SPD-



Reagents and conditions: (a) 1,3-dibromopropane,  $K_2CO_3$ , DMF (b) (1)  $ClSO_3H$  (2)  $NH_3 \cdot H_2O$ , THF (c) (1)  $NaOMe$ , MeOH, (2) 4-isocyanato-1,2,3,5,6,7-hexahydro-s-indacene, MeCN.

Reagents and conditions: (a) hexachloroethane,  $PPh_3$ , DCM (b)  $LiBH_4$ , EtOH (c)  $PPh_3$ , 1-acetyl-1,2-dihydro-3H-pyrazol-3-one, DIAD, THF (d)  $K_2CO_3$ , MeOH, MeCN (e)  $NaH$ ,  $MeI$ ,  $Et_3N$ , DMF (f) (1)  $HCl/dioxane$ , DCM, (2) TFAA, TFA, DCM; (g) (1)  $ClSO_3H$ , DCM, (2) pyridine, (3)  $PCl_5$ , (4)  $NH_3$  gas in THF; (h) (1)  $NaH$ , MeOH, (2) 4-isocyanato-1,2,3,5,6,7-hexahydro-s-indacene, MeCN; (i)  $NaOH$ .

**Figure 13.** Synthesis of Compounds 17 and GDC-2394 (20).

M30A UV detector, a CTO-20A column oven, using a 2–98% acetonitrile/0.1% formic acid (or 0.001% ammonia) gradient over 2.5 min. Flash column chromatography purifications were performed on a Teledyne Isco CombiFlash  $R_f$  utilizing Silicycle HP columns using a mobile phase composed of either heptane/isopropyl acetate or dichloromethane/methanol. All final compounds were purified to have purity higher than 95% by reverse-phase high-performance liquid chromatography (HPLC), or normal-phase silica gel flash chromatography. Purity determination and retention times ( $R_t$ ) were determined using the following method: A UPLC-CAD-MS system (Agilent Infinity II LC-MSD iQ) was utilized to measure percent purity and concentration of DMSO samples. The chromatography conditions utilized a Waters Acuity BEH C18 column (2.1 mm × 50 mm, 1.7  $\mu$ m particle size) and mobile phase A (water with 0.1% formic acid) with mobile phase B (Methanol). A 3 min gradient utilized with the following details: starting with 2% B for 15 s; 2–98% B over 2 min; hold 98% B for 30 s; 2% B for 15 s. The flow rate was 0.40 mL/min, column temperature was 40 °C, and UV absorbance data were collected at 254 nm. HPLC traces for all compounds with in vivo data are available in the Supporting Information.

**4-Isocyanato-1,2,3,5,6,7-hexahydro-s-indacene.** Triphosgene (0.33 equiv) was added to a solution of 1,2,3,5,6,7-hexahydro-s-indacen-4-ylamine (1 equiv) and TEA (1.1 equiv) in THF (0.3 M) at 0 °C. After 5 min, the reaction mixture was heated at 70 °C for 1 h. The reaction mixture was cooled to room temperature and was filtered through a pad of silica gel plug using hexane. The filtrate was concentrated under reduced pressure to give 4-isocyanato-1,2,3,5,6,7-hexahydro-s-indacene which was used in the next step without further purification.

**General Procedure for the Preparation of Sulfonylureas 2–16.** Sodium hydroxide (10 mass% in water, 1.0 equiv) was added to a solution of sulfonamide (1.0 equiv) in acetone (0.3 M), and the reaction mixture was heated at 70 °C in an open vial for 5 min (or until all the solvent was removed). The reaction mixture was cooled to room temperature, and the flask was placed under high vacuum to remove any remaining acetone/water. The crude residue was then

dissolved in acetone (0.3 M), and the reaction mixture was heated at 70 °C. A solution of 4-isocyanato-1,2,3,5,6,7-hexahydro-s-indacene (1 equiv) in acetone (0.3 M) was added dropwise to the solution over 1 min. After addition, the reaction continued heating at 70 °C until no solvent remained. The crude residue was purified by reverse-phase HPLC to deliver the desired sulfonylurea.

***N*-(1,2,3,5,6,7-Hexahydro-s-indacen-4-yl)carbamoylfuran-2-sulfonamide Sodium Salt (2).**  $^1H$  NMR (400 MHz,  $DMSO-d_6$ )  $\delta$  7.62 (t,  $J = 1.4$  Hz, 1H), 7.55 (s, 1H), 6.78 (s, 1H), 6.60 (d,  $J = 3.3$  Hz, 1H), 6.44 (dd,  $J = 3.3$ , 1.8 Hz, 1H), 2.75 (t,  $J = 7.4$  Hz, 4H), 2.65 (t,  $J = 7.4$  Hz, 4H), 1.90 (p,  $J = 7.4$  Hz, 4H). LCMS ( $m/z$ ): 347.1 (M +  $H^+$ ),  $R_t$  4.99 min.

***N*-(1,2,3,5,6,7-Hexahydro-s-indacen-4-yl)carbamoylbenzenesulfonamide (3).**  $^1H$  NMR (400 MHz,  $DMSO-d_6$ )  $\delta$  10.78 (bs, 1H), 8.08 (s, 1H), 7.98–7.90 (m, 2H), 7.73–7.65 (m, 1H), 7.65–7.53 (m, 2H), 6.92 (s, 1H), 2.76 (t,  $J = 7.4$  Hz, 4H), 2.53 (d,  $J = 7.3$  Hz, 4H), 1.91 (p,  $J = 7.4$  Hz, 4H). LCMS ( $m/z$ ): 357.1 (M +  $H^+$ ),  $R_t$  5.25 min.

***N*-(1,2,3,5,6,7-Hexahydro-s-indacen-4-yl)carbamoylpyridine-2-sulfonamide (4).**  $^1H$  NMR (400 MHz,  $DMSO-d_6$ )  $\delta$  10.94 (bs, 1H), 8.76 (dt,  $J = 4.7$ , 1.4 Hz, 1H), 8.17–8.06 (m, 2H), 8.09–8.01 (m, 1H), 7.71 (ddd,  $J = 7.5$ , 4.7, 1.2 Hz, 1H), 6.92 (s, 1H), 2.76 (t,  $J = 7.4$  Hz, 4H), 2.54 (t,  $J = 7.3$  Hz, 4H), 1.92 (p,  $J = 7.5$  Hz, 4H). LCMS ( $m/z$ ): 358.1 (M +  $H^+$ ),  $R_t$  4.76 min.

***N*-(1,2,3,5,6,7-Hexahydro-s-indacen-4-yl)carbamoylpyridine-3-sulfonamide (5).**  $^1H$  NMR (400 MHz,  $DMSO-d_6$ )  $\delta$  10.84 (bs, 1H), 9.07 (d,  $J = 2.3$  Hz, 1H), 8.86 (dd,  $J = 4.9$ , 1.6 Hz, 1H), 8.32 (dt,  $J = 8.1$ , 2.0 Hz, 1H), 8.27 (s, 1H), 7.67 (dd,  $J = 8.1$ , 4.8 Hz, 1H), 6.93 (s, 1H), 2.77 (t,  $J = 7.4$  Hz, 4H), 2.53 (d,  $J = 7.3$  Hz, 4H), 1.91 (p,  $J = 7.5$  Hz, 4H). LCMS ( $m/z$ ): 358.1 (M +  $H^+$ ),  $R_t$  4.54 min.

***N*-(1,2,3,5,6,7-Hexahydro-s-indacen-4-yl)carbamoylpyridine-4-sulfonamide (6).**  $^1H$  NMR (400 MHz,  $DMSO-d_6$ )  $\delta$  11.13 (bs, 1H), 8.93–8.87 (m, 2H), 8.33 (s, 1H), 7.90–7.83 (m, 2H), 6.94 (s, 1H), 2.77 (t,  $J = 7.3$  Hz, 4H), 2.54 (t,  $J = 7.3$  Hz, 4H), 1.92 (p,  $J = 7.5$  Hz, 4H). LCMS ( $m/z$ ): 358.1 (M +  $H^+$ ),  $R_t$  4.52 min.

*N*-(*1,2,3,5,6,7-Hexahydro-s-indacen-4-yl*)carbamoyl)pyrazine-2-sulfonamide Sodium Salt (**7**). <sup>1</sup>H NMR (400 MHz, DMSO-d<sub>6</sub>) δ 9.12 (dd, *J* = 6.5, 1.5 Hz, 1H), 8.81 (d, *J* = 2.4 Hz, 1H), 8.76 (d, *J* = 2.1 Hz, 1H), 7.90 (bs, 1H), 6.85 (s, 1H), 2.75 (t, *J* = 7.3 Hz, 4H), 2.57 (t, *J* = 7.4 Hz, 4H), 1.96–1.84 (m, 4H). LCMS (*m/z*): 359.1 (M + H<sup>+</sup>), *R*<sub>t</sub> 4.57 min.

*N*-(*1,2,3,5,6,7-Hexahydro-s-indacen-4-yl*)carbamoyl)thiazole-2-sulfonamide Sodium Salt (**8**). <sup>1</sup>H NMR (400 MHz, DMSO-d<sub>6</sub>) δ 7.93–7.86 (m, 1H), 7.76–7.69 (m, 1H), 7.59 (s, 1H), 6.77 (s, 1H), 2.74 (t, *J* = 7.4 Hz, 4H), 2.66 (t, *J* = 7.3 Hz, 4H), 1.89 (p, *J* = 7.4 Hz, 4H). LCMS (*m/z*): 364.1 (M + H<sup>+</sup>), *R*<sub>t</sub> 4.84 min.

*N*-(*1,2,3,5,6,7-Hexahydro-s-indacen-4-yl*)carbamoyl)-2-methyl-thiazole-5-sulfonamide Sodium Salt (**9**). <sup>1</sup>H NMR (400 MHz, DMSO-d<sub>6</sub>) δ 7.71 (s, 1H), 7.45 (s, 1H), 6.78 (s, 1H), 2.75 (t, *J* = 7.4 Hz, 4H), 2.66 (t, *J* = 7.4 Hz, 4H), 2.59 (s, 3H), 1.90 (p, *J* = 7.4 Hz, 4H). LCMS (*m/z*): 378.0 (M + H<sup>+</sup>), *R*<sub>t</sub> 4.83 min.

*N*-(*1,2,3,5,6,7-Hexahydro-s-indacen-4-yl*)carbamoyl)-1,2-dimethyl-1*H*-imidazole-4-sulfonamide Sodium Salt (**10**). <sup>1</sup>H NMR (400 MHz, DMSO-d<sub>6</sub>) δ 7.64 (s, 1H), 7.21 (s, 1H), 6.77 (s, 1H), 3.52 (s, 3H), 2.75 (t, *J* = 7.4 Hz, 4H), 2.66 (t, *J* = 7.4 Hz, 4H), 2.24 (s, 3H), 1.96–1.85 (m, 4H). LCMS (*m/z*): 375.1 (M + H<sup>+</sup>), *R*<sub>t</sub> 4.29 min.

*N*-(*1,2,3,5,6,7-Hexahydro-s-indacen-4-yl*)carbamoyl)-1-methyl-1*H*-pyrazole-5-sulfonamide Sodium Salt (**11**). <sup>1</sup>H NMR (400 MHz, DMSO-d<sub>6</sub>) δ 7.68 (s, 1H), 7.33 (d, *J* = 1.9 Hz, 1H), 6.81 (s, 1H), 6.46 (d, *J* = 1.9 Hz, 1H), 3.98 (s, 3H), 2.75 (t, *J* = 7.4 Hz, 4H), 2.63 (t, *J* = 7.4 Hz, 4H), 1.98–1.85 (m, 4H). LCMS (*m/z*): 361.1 (M + H<sup>+</sup>), *R*<sub>t</sub> 4.79 min.

*N*-(*1,2,3,5,6,7-Hexahydro-s-indacen-4-yl*)carbamoyl)-1-methyl-1*H*-pyrazole-3-sulfonamide (**12**). <sup>1</sup>H NMR (400 MHz, DMSO-d<sub>6</sub>) δ 10.79 (bs, 1H), 8.02 (s, 1H), 7.89 (d, *J* = 2.3 Hz, 1H), 6.94 (s, 1H), 6.73 (d, *J* = 2.3 Hz, 1H), 3.93 (s, 3H), 2.79 (t, *J* = 7.4 Hz, 4H), 2.60 (t, *J* = 7.4 Hz, 4H), 1.95 (p, *J* = 7.4 Hz, 4H). LCMS (*m/z*): 361.1 (M + H<sup>+</sup>), *R*<sub>t</sub> 4.60 min.

*N*-(*1,2,3,5,6,7-Hexahydro-s-indacen-4-yl*)carbamoyl)-1-methyl-1*H*-pyrazole-4-sulfonamide (**13**). <sup>1</sup>H NMR (400 MHz, DMSO-d<sub>6</sub>) δ 10.56 (bs, 1H), 8.37 (s, 1H), 8.01 (s, 1H), 7.83 (s, 1H), 6.94 (s, 1H), 3.88 (s, 3H), 2.79 (t, *J* = 7.4 Hz, 4H), 2.59 (t, *J* = 7.3 Hz, 4H), 1.95 (p, *J* = 7.5 Hz, 4H). LCMS (*m/z*): 361.1 (M + H<sup>+</sup>), *R*<sub>t</sub> 4.44 min.

*N*-(*1,2,3,5,6,7-Hexahydro-s-indacen-4-yl*)carbamoyl)-1-isopropyl-1*H*-pyrazole-4-sulfonamide Sodium Salt (**14**). <sup>1</sup>H NMR (400 MHz, DMSO-d<sub>6</sub>) δ 8.09 (s, 1H), 7.64 (s, 1H), 7.56 (s, 1H), 6.82 (s, 1H), 4.53–5.47 (m, 1H), 2.76 (t, *J* = 7.4 Hz, 4H), 2.61 (t, *J* = 7.4 Hz, 4H), 1.91 (p, *J* = 7.4 Hz, 4H), 1.39 (d, *J* = 6.7 Hz, 6H). LCMS (*m/z*): 389.2 (M + H<sup>+</sup>), *R*<sub>t</sub> 5.01 min.

*N*-(*1,2,3,5,6,7-Hexahydro-s-indacen-4-yl*)carbamoyl)-1,5-dimethyl-1*H*-pyrazole-4-sulfonamide (**15**). <sup>1</sup>H NMR (400 MHz, DMSO-d<sub>6</sub>) δ 10.54 (s, 1H), 7.99 (s, 1H), 7.79 (s, 1H), 6.94 (s, 1H), 4.09 (t, *J* = 5.6 Hz, 2H), 2.97 (t, *J* = 6.4 Hz, 2H), 2.78 (t, *J* = 7.6 Hz, 4H), 2.57 (t, *J* = 7.6 Hz, 4H), 1.98–1.90 (m, 6H), 1.82–1.78 (m, 2H). LCMS (*m/z*): 401.0 (M + H<sup>+</sup>).

*N*-(*1,2,3,5,6,7-Hexahydro-s-indacen-4-yl*)carbamoyl)-4,5,6,7-tetrahydropyrazolo[1,5-a]pyridine-3-sulfonamide (**16**). <sup>1</sup>H NMR (400 MHz, DMSO-d<sub>6</sub>) δ 10.54 (s, 1H), 7.99 (s, 1H), 7.79 (s, 1H), 6.94 (s, 1H), 4.09 (t, *J* = 5.6 Hz, 2H), 2.97 (t, *J* = 6.4 Hz, 2H), 2.78 (t, *J* = 7.6 Hz, 4H), 2.57 (t, *J* = 7.6 Hz, 4H), 1.98–1.90 (m, 6H), 1.82–1.78 (m, 2H). MS: *m/z* 401.0 (M + H<sup>+</sup>).

*N*-(*1,2,3,5,6,7-Hexahydro-s-indacen-4-yl*)carbamoyl)-6,7-dihydro-5*H*-pyrazolo[5,1-b][1,3]oxazine-3-sulfonamide Sodium Salt (**17**). 1,2-Dihydro-pyrazol-3-one (53.0 g, 630.9 mmol) and K<sub>2</sub>CO<sub>3</sub> (305.0 g, 2210.1 mmol) were heated to 130 °C in DMF (1 L). Then, 1,3-dibromopropane (140.0 g, 693.1 mmol) was added. After 8 h, the reaction mixture was cooled to room temperature and concentrated under reduced pressure. The residue was partitioned between ethyl acetate (200 mL) and water (500 mL), and the layers were separated. The aqueous layer was extracted with ethyl acetate (150 mL × 8). The combined organic layers were washed with brine (300 mL), dried over Na<sub>2</sub>SO<sub>4</sub>, filtered, and concentrated in vacuo. The crude residue was purified by silica gel column chromatography (petroleum ether/ethyl acetate = 3/1) to give 6,7-dihydro-5*H*-pyrazolo[5,1-b][1,3]-oxazine (64.0 g, yield: 41%) as a yellow oil. <sup>1</sup>H NMR (400 MHz,

CDCl<sub>3</sub>) δ 7.31 (d, *J* = 2.0 Hz, 1H), 5.48 (d, *J* = 2.0 Hz, 1H), 4.28 (t, *J* = 5.2 Hz, 2H), 4.18 (t, *J* = 6.2 Hz, 2H), 2.29–2.22 (m, 2H).

6,7-Dihydro-5*H*-pyrazolo[5,1-b][1,3]oxazine (64.0 g, 516.1 mmol) was added dropwise to ClSO<sub>3</sub>H (380 mL) at 0 °C. The reaction mixture was then heated to 80 °C. After 16 h, the reaction mixture was added dropwise to a mixture of ice water/ethyl acetate (4 L/1.5 L). The layers were separated, and the aqueous layer was extracted with ethyl acetate (300 mL × 2). The combined organic layers were washed with brine (500 mL), dried over Na<sub>2</sub>SO<sub>4</sub>, and concentrated in vacuo. The crude residue was washed with petroleum ether (200 mL) to give 6,7-dihydro-5*H*-pyrazolo[5,1-b][1,3]oxazine-3-sulfonyl chloride (73.0 g, yield: 63%) as a yellow solid.

To a solution of 6,7-dihydro-5*H*-pyrazolo[5,1-b][1,3]oxazine-3-sulfonyl chloride (73.0 g, 328.8 mmol) in THF (430 mL) was added NH<sub>3</sub>•H<sub>2</sub>O (180 mL) at room temperature. The reaction mixture was heated at 60 °C. After 16 h, the reaction mixture was concentrated to dryness. The crude residue was washed with 0.2 M aqueous HCl (110 mL) and H<sub>2</sub>O (40 mL) and dried to give 6,7-dihydro-5*H*-pyrazolo[5,1-b][1,3]oxazine-3-sulfonic acid amide (52.0 g, yield: 78%) as a yellow solid.

<sup>1</sup>H NMR (300 MHz, DMSO-d<sub>6</sub>): δ = 7.47 (s, 1H), 7.08 (s, 2H), 4.40 (t, *J* = 5.1 Hz, 2H), 4.10 (t, *J* = 6.0 Hz, 2H), 2.23–2.15 (m, 2H). LCMS (*m/z*): 203.9 (M + H<sup>+</sup>).

A suspension of 6,7-dihydro-5*H*-pyrazolo[5,1-b][1,3]oxazine-3-sulfonic acid amide (14.3 g, 70.4 mmol) was dissolved in MeOH (500 mL) at 80 °C, and then NaOMe (3.8 g, 70.4 mmol) was added. After 5 min, the reaction mixture was cooled to room temperature and concentrated to dryness. The crude residue was coevaporated with MeCN (100 mL). The residual solid was suspended in MeCN (320 mL) at room temperature, and 4-isocyanato-1,2,3,5,6,7-hexahydro-s-indacene (14.6 g, 73.3 mmol) was added. After 16 h, the reaction mixture was filtered. The filter cake was triturated with EtOH (250 mL) and then petroleum ether/ethyl acetate (5/1, 250 mL). The residue was then dissolved in water (200 mL) and concentrated to dryness to give *N*-(*1,2,3,5,6,7-hexahydro-s-indacen-4-yl*)carbamoyl)-6,7-dihydro-5*H*-pyrazolo[5,1-b][1,3]oxazine-3-sulfonamide as a sodium salt (24.5 g, yield: 82%) as a white solid. <sup>1</sup>H NMR (400 MHz, D<sub>2</sub>O) δ 7.64 (s, 1H), 7.02 (s, 1H), 4.40 (t, *J* = 5.2 Hz, 2H), 4.11 (t, *J* = 6.0 Hz, 2H), 2.83 (t, *J* = 7.2 Hz, 4H), 2.66 (t, *J* = 7.2 Hz, 4H), 2.28–2.22 (m, 2H), 2.04–1.96 (m, 4H). LCMS (*m/z*): 403.1 (M + H<sup>+</sup>).

*N*-(*1,2,3,5,6,7-Hexahydro-s-indacen-4-yl*)carbamoyl)pyrazolo[1,5-a]pyrimidine-3-sulfonamide Sodium Salt (**18**). The title compound was prepared analogously to *N*-(*1,2,3,5,6,7-hexahydro-s-indacen-4-yl*)carbamoyl)-6,7-dihydro-5*H*-pyrazolo[5,1-b][1,3]-oxazine-3-sulfonamide, specifically by substituting 6,7-dihydro-5*H*-pyrazolo[5,1-b][1,3]oxazine-3-sulfonamide with pyrazolo[1,5-a]pyrimidine-3-sulfonyl chloride. <sup>1</sup>H NMR (400 MHz, DMSO-d<sub>6</sub>) δ 9.13 (dd, *J* = 7.0, 1.8 Hz, 1H), 8.61 (dd, *J* = 4.1, 1.7 Hz, 1H), 8.25 (s, 1H), 7.42 (s, 1H), 7.11 (dd, *J* = 7.0, 4.1 Hz, 1H), 6.74 (s, 1H), 2.73 (dt, *J* = 14.5, 7.3 Hz, 4H), 2.56 (t, *J* = 7.3 Hz, 4H), 1.95–1.85 (m, 4H). LCMS (*m/z*): 398.1 (M + H<sup>+</sup>), *R*<sub>t</sub> 4.41 min.

*N*-(*1,2,3,5,6,7-Hexahydro-s-indacen-4-yl*)carbamoyl)-5-methyl-4-oxo-4,5,6,7-tetrahydropyrazolo[1,5-a]pyrimidine-3-sulfonamide (**19**). To a solution of 4-nitro-1*H*-pyrazole-5-carboxylic acid (1.0 g, 6.4 mmol) and 2-(methylamino)ethanol (0.55 g, 7.3 mmol) in toluene (5 mL) were added SOCl<sub>2</sub> (20 mL) and DMF (3 drops) at -5 °C. After 10 min, the reaction mixture was heated to 80 °C and was allowed to stir overnight. The reaction mixture was concentrated in vacuo. The crude residue was dissolved in DMF (20 mL) and triethylamine (2.7 mL, 19.3 mmol) and was heated at 60 °C overnight. The reaction mixture was concentrated in vacuo, and the crude residue was purified by silica gel column chromatography (petroleum ether/ethyl acetate = 3/1~1/1) to give 5-methyl-3-nitro-6,7-dihydropyrazolo[1,5-a]-pyrimin-4(5*H*)-one (0.7 g, 56%) as a yellow solid. <sup>1</sup>H NMR (400 MHz, DMSO-d<sub>6</sub>) δ 8.34 (s, 1H), 4.47 (t, *J* = 5.6 Hz, 2H), 3.85 (t, *J* = 6.4 Hz, 2H), 3.05 (s, 3H).

To a solution of 5-methyl-3-nitro-6,7-dihydropyrazolo[1,5-a]-pyrimin-4(5*H*)-one (3.52 g, 18 mmol) in EtOH (75 mL) were added iron powder (5.04 g, 90 mmol), NH<sub>4</sub>Cl (4.82 g, 90 mmol), and

$\text{H}_2\text{O}$  (25 mL). The reaction mixture was heated to 80 °C. After 12 h, the reaction mixture was filtered, and the filtrate was concentrated in vacuo. The crude residue was purified by silica gel column chromatography (dichloromethane/MeOH = 10/1) to give 3-amino-5-methyl-6,7-dihydropyrazolo[1,5-*a*]pyrazin-4(5*H*)-one (2.58 g, 86%) as a yellow solid.  $^1\text{H}$  NMR (400 MHz, DMSO- $d_6$ )  $\delta$  7.01 (s, 1H), 4.76 (s, 2H), 4.16 (t,  $J$  = 6.0 Hz, 2H), 3.66 (t,  $J$  = 6.4 Hz, 2H), 2.94 (s, 3H).

$\text{SOCl}_2$  (20 mL) was added dropwise to water (70 mL) at -5 °C. After 1 h, the reaction mixture was warmed to room temperature and was allowed to stir for an additional 1 h. Copper(I) chloride (0.16 g, 1.11 mmol) was added to give a yellow solution. After 5 min, the reaction mixture was cooled to -10 °C. In a separate flask, a solution of  $\text{NaNO}_2$  (180 mg, 2.62 mmol) in water (1.6 mL) was added dropwise to a solution of 3-amino-5-methyl-6,7-dihydropyrazolo[1,5-*a*]pyrazin-4(5*H*)-one (358 mg, 2.2 mmol) in conc. HCl (2.0 mL) at -10 °C. The resulting dark orange solution was stirred at -10 °C for 30 min and then was added dropwise to the above solution of copper(I) chloride (5.7 mL) at -5 °C over 5 min. After 1 h, the reaction mixture was poured into a separatory funnel, and the aqueous layer was extracted with ethyl acetate (5 mL  $\times$  3). The organic layer was concentrated in vacuo to give a yellow solid. The solid was dissolved in THF (5 mL), and  $\text{NH}_3$  (3 mL, 28 wt %) was added dropwise at -5 °C. After 2 h, the reaction mixture was concentrated in vacuo. The crude residue was purified by prep-TLC (dichloromethane/MeOH = 10/1) to give 5-methyl-4-oxo-4,5,6,7-tetrahydropyrazolo[1,5-*a*]pyrazine-3-sulfonamide (30 mg, 6%) as a yellow solid.  $^1\text{H}$  NMR (400 MHz, DMSO- $d_6$ )  $\delta$  7.86 (s, 1H), 7.18 (s, 2H), 4.48 (t,  $J$  = 6.0 Hz, 2H), 3.87 (t,  $J$  = 6.4 Hz, 2H), 3.06 (s, 3H).

Sodium hydride (6.24 mg, 0.156 mmol, 60% dispersion in paraffin liquid) in DMSO (2 mL) was stirred at 70 °C. After 30 min, a solution of 5-methyl-4-oxo-4,5,6,7-tetrahydropyrazolo[1,5-*a*]pyrazine-3-sulfonamide (30 mg, 0.13 mmol) in DMSO (2 mL) was added at -5 °C. The reaction mixture was allowed to stir for an additional 30 min at which point a solution of 4-isocyanato-1,2,3,5,6,7-hexahydro-s-indacene (0.14 mmol) in THF (5 mL) was added. The reaction temperature was warmed to room temperature. After 12 h, saturated aqueous ammonium chloride was added, and the reaction mixture was diluted with ethyl acetate. The organic layer was washed with saturated aqueous ammonium chloride (5 mL  $\times$  3), dried over anhydrous  $\text{Na}_2\text{SO}_4$ , and concentrated in vacuo. The crude residue was purified by prep-HPLC to give *N*-(1,2,3,5,6,7-hexahydro-s-indacen-4-yl)carbamoyl)-5-methyl-4-oxo-4,5,6,7-tetrahydropyrazolo[1,5-*a*]pyrazine-3-sulfonamide (12.8 mg, 25%) as a white solid.  $^1\text{H}$  NMR (400 MHz, DMSO- $d_6$ )  $\delta$  8.27 (brs, 1H), 7.91 (s, 1H), 6.90 (s, 1H), 4.47 (t,  $J$  = 5.6 Hz, 2H), 3.83 (t,  $J$  = 6.0 Hz, 2H), 3.06 (s, 3H), 2.77 (t,  $J$  = 6.8 Hz, 4H), 2.55 (t,  $J$  = 7.6 Hz, 4H), 1.99–1.88 (m, 4H). MS:  $m/z$  430.1 ( $M + \text{H}^+$ ).

(*S*)-*N*-(1,2,3,5,6,7-hexahydro-s-indacen-4-yl)carbamoyl)-6-(methylamino)-6,7-dihydro-5*H*-pyrazolo[5,1-*b*][1,3]oxazine-3-sulfonamide Sodium Salt (**20**). To a solution of (*S*)-methyl 2-((tert-butoxycarbonyl)amino)-3-hydroxypropanoate (100 g, 457 mmol) in DCM (1.8 L) were added  $\text{PPh}_3$  (132 g, 504 mmol) and hexachloroethane (119 g, 504 mmol) at room temperature. After 3 h, saturated aqueous  $\text{NaHCO}_3$  was added to adjust the pH of the reaction mixture to pH = 8. The organic phase was separated, dried with  $\text{Na}_2\text{SO}_4$ , and concentrated under reduced pressure. The crude residue was triturated with petroleum ether/ethyl acetate (5/1, 1000 mL), filtered, and concentrated under reduced pressure. The crude residue was purified by silica gel column chromatography (petroleum ether/ethyl acetate = 6/1) to give (*R*)-methyl 2-((tert-butoxycarbonyl)amino)-3-chloropropanoate (78.3 g, yield: 72%) as a white solid.

$\text{LiBH}_4$  (2 M in THF, 170 mL, 340 mmol) was added dropwise to a solution of (*R*)-methyl 2-((tert-butoxycarbonyl)amino)-3-chloropropanoate (78.3 g, 330 mmol) in ethanol (1.5 L) at 0 °C. The reaction mixture was allowed to warm to room temperature over 1 h. After an additional 1 h, saturated aqueous  $\text{NH}_4\text{Cl}$  (250 mL) was added. The organics were evaporated under reduced pressure. The crude residue was partitioned between water (200 mL) and ethyl acetate (500 mL).

The organic layer was separated, and the aqueous layer was further extracted with ethyl acetate (200 mL). The combined organic layers were washed with brine (100 mL), dried with  $\text{NaSO}_4$ , and concentrated under reduced pressure. The crude residue was purified by silica gel column chromatography (petroleum ether/ethyl acetate (10/1) to ethyl acetate) to give (*R*)-tert-butyl (1-chloro-3-hydroxypropan-2-yl)carbamate (66.4 g, yield: 96%) as a white solid.  $^1\text{H}$  NMR (400 MHz,  $\text{CDCl}_3$ )  $\delta$  5.04 (d,  $J$  = 7.2 Hz, 1H), 3.93 (brs, 1H), 3.87–3.81 (m, 1H), 3.78–3.65 (m, 3H), 2.37 (brs, 1H), 1.45 (s, 9H).

DIAD (79 mL, 400 mmol) was added dropwise to a suspension of 1-acetyl-1*H*-pyrazol-3(2*H*)-one (38.8 g, 308.4 mmol), (*R*)-tert-butyl (1-chloro-3-hydroxypropan-2-yl)carbamate (66.4 g, 318 mmol) and  $\text{PPh}_3$  (105 g, 401 mmol) in THF (500 mL) dropwise at 0 °C. The reaction mixture was warmed to room temperature and was allowed to stir for 16 h. The reaction mixture was concentrated under reduced pressure. The crude residue was triturated with petroleum ether/ethyl acetate (5/1, 1000 mL), filtered, and concentrated under reduced pressure. The crude residue was purified by silica gel column chromatography (petroleum ether/ethyl acetate = 15/1 to 10/1) to give (*R*)-tert-butyl (1-((1-acetyl-1*H*-pyrazol-3-yl)oxy)-3-chloropropan-2-yl)carbamate (66.1 g, yield: 68%) as a colorless oil.

A mixture of (*R*)-tert-butyl (1-((1-acetyl-1*H*-pyrazol-3-yl)oxy)-3-chloropropan-2-yl)carbamate (66 g, 209 mmol) and  $\text{K}_2\text{CO}_3$  (86 g, 623 mmol) in MeOH/MeCN (40 mL/2000 mL) was refluxed at 85 °C. After 20 h, the reaction mixture was filtered, and the filtrate was concentrated under reduced pressure. The crude residue was triturated with petroleum ether/ethyl acetate (3/1, 250 mL) and filtered to give (*S*)-tert-butyl (6,7-dihydro-5*H*-pyrazolo[5,1-*b*][1,3]-oxazin-6-yl)carbamate (40.3 g, yield: 81%) as a white solid.  $^1\text{H}$  NMR (400 MHz,  $\text{CDCl}_3$ )  $\delta$  7.36 (d,  $J$  = 2.0 Hz, 1H), 5.54 (d,  $J$  = 2.0 Hz, 1H), 5.08 (d,  $J$  = 7.2 Hz, 1H), 4.36 (brs, 1H), 4.33–4.27 (m, 2H), 4.23–4.18 (m, 2H), 1.45 (s, 9H).

To a solution of (*S*)-tert-butyl (6,7-dihydro-5*H*-pyrazolo[5,1-*b*][1,3]oxazin-6-yl)carbamate (40.3 g, 169 mmol) and  $\text{Et}_3\text{N}$  (36 mL, 253 mmol) in DMF (500 mL) was added NaH (60% in mineral oil, 10.1 g, 253 mmol) portion-wise at 0 °C. After 30 min, iodomethane (21.0 mL, 337 mmol) was added dropwise at 0 °C. The reaction mixture was warmed to room temperature. After 2 h, the reaction mixture was poured into water (1500 mL). The aqueous layer was extracted with ethyl acetate (500 mL  $\times$  3). The combined organic layers were washed with brine (1000 mL  $\times$  3), dried over  $\text{Na}_2\text{SO}_4$ , and concentrated under reduced pressure. The crude residue was purified by silica gel column chromatography (petroleum ether/ethyl acetate = 2/1) to give (*S*)-tert-butyl (6,7-dihydro-5*H*-pyrazolo[5,1-*b*][1,3]oxazin-6-yl)(methyl)carbamate (41.0 g, yield: 96%) as a white solid.

To a solution of (*S*)-tert-butyl (6,7-dihydro-5*H*-pyrazolo[5,1-*b*][1,3]oxazin-6-yl)(methyl)carbamate (10.0 g, 39.5 mmol) in DCM (50 mL) was added HCl/dioxane (6 M, 100 mL) at room temperature. After 3 h, the reaction mixture was concentrated under reduced pressure. The crude residue was suspended in DCM (100 mL) cooled to 0 °C.  $\text{Et}_3\text{N}$  (22 mL, 157 mmol) and TFAA (6.7 mL, 47.4 mmol) were added dropwise. The reaction mixture was warmed to room temperature. After 1 h, the reaction mixture was diluted with DCM (100 mL). The organic layer was washed with water (100 mL), saturated aqueous  $\text{NaHCO}_3$  (50 mL), and brine (50 mL), dried over  $\text{Na}_2\text{SO}_4$ , and concentrated under reduced pressure to give (*S*)-*N*-(6,7-dihydro-5*H*-pyrazolo[5,1-*b*][1,3]oxazin-6-yl)-2,2,2-trifluoro-N-methylacetamide (9.0 g, yield: 91%) as a yellow oil.  $^1\text{H}$  NMR (400 MHz,  $\text{CDCl}_3$ )  $\delta$  7.39 (d,  $J$  = 2.0 Hz, 1H), 5.56 (d,  $J$  = 2.0 Hz, 1H), 5.05–5.01 (m, 1H), 4.56–4.46 (m, 2H), 4.37–4.31 (m, 2H), 3.07–3.02 (m, 3H).

To a solution of (*S*)-*N*-(6,7-dihydro-5*H*-pyrazolo[5,1-*b*][1,3]oxazin-6-yl)-2,2,2-trifluoro-N-methylacetamide (9.8 g, 39.4 mmol) in DCM (100 mL) was added  $\text{ClSO}_3\text{H}$  (6.5 mL, 97.9 mmol) dropwise at 0 °C. The mixture was refluxed at 45 °C for 2 h. The reaction mixture was cooled to 0 °C. Pyridine (7.8 mL, 97.9 mmol) was added dropwise, and then  $\text{PCl}_5$  (20.3 g, 97.9 mmol) was added portion-wise. The reaction mixture was then refluxed at 45 °C. After 1

h, the reaction mixture was cooled to room temperature and was allowed to stir at this temperature for an additional 16 h. The reaction mixture was poured carefully into ice water (300 mL). The aqueous layer was extracted with ethyl acetate (100 mL  $\times$  2). The combined organic layers were washed with brine (100 mL), dried over  $\text{Na}_2\text{SO}_4$ , and concentrated under reduced pressure. The crude residue was purified by silica gel column chromatography (petroleum ether/ethyl acetate = 2/1) to give (*S*)-6-(2,2,2-trifluoro-N-methylacetamido)-6,7-dihydro-5H-pyrazolo[5,1-*b*][1,3]oxazine-3-sulfonyl chloride (6.7 g, yield: 49%) as a yellow solid.

$\text{NH}_3$  (gas) was bubbled through a solution of (*S*)-6-(2,2,2-trifluoro-N-methylacetamido)-6,7-dihydro-5H-pyrazolo[5,1-*b*][1,3]oxazine-3-sulfonyl chloride (36.3 g, 105 mmol) in THF (300 mL) for 10 min at 0 °C. Then, the reaction mixture was warmed to room temperature and stirred for an additional 2 h. Concentrated HCl was added to the reaction to adjust the pH to 3~4. The suspension was filtered, and the filtrate was concentrated under reduced pressure. The crude residue was purified by silica gel column chromatography (DCM/MeOH = 20/1) to give (*S*)-2,2,2-trifluoro-N-methyl-N-(3-sulfamoyl)-6,7-dihydro-5H-pyrazolo[5,1-*b*][1,3]oxazin-6-yl)acetamide (25.0 g, yield: 73%) as a yellow solid.  $^1\text{H}$  NMR (400 MHz, DMSO- $d_6$ )  $\delta$  7.58 (s, 1H), 7.19 (s, 2H), 5.00–4.90 (m, 1H), 4.70–4.55 (m, 2H), 4.54–4.40 (m, 2H), 3.05–2.93 (m, 3H).

To a solution of (*S*)-2,2,2-trifluoro-N-methyl-N-(3-sulfamoyl)-6,7-dihydro-5H-pyrazolo[5,1-*b*][1,3]oxazin-6-yl)acetamide (5.0 g, 15.2 mmol) in THF (50 mL) was added NaH (610 mg, 15.2 mmol) in small portions at 0 °C. After 20 min, 4-isocyanato-1,2,3,5,6,7-hexahydro-s-indacene (3.03 g, 15.2 mmol) was added, and the reaction mixture was warmed to room temperature. After 2 h,  $\text{H}_2\text{O}$  (50 mL) and NaOH (1.22 g, 30.4 mmol) were added, and the reaction mixture was stirred at room temperature for an additional 30 min. The reaction mixture was concentrated under reduced pressure, to remove the THF, and filtered to remove the insoluble solid. The aqueous layer was washed with ethyl acetate (15 mL). Then concentrated HCl was added to the aqueous layer to adjust the pH to 9. The solution was filtered, and the crude material was purified by reverse-phase column (5~40% MeCN in  $\text{H}_2\text{O}$ ) to give ((*S*)-*N*-((1,2,3,5,6,7-hexahydro-s-indacen-4-yl)carbamoyl)-6-(methylamino)-6,7-dihydro-5H-pyrazolo[5,1-*b*][1,3]oxazine-3-sulfonamide sodium salt (5.6 g, yield: 85%) as a white solid.  $^1\text{H}$  NMR (400 MHz, DMSO- $d_6$ )  $\delta$  7.42 (s, 1H), 7.34 (s, 1H), 6.76 (s, 1H), 4.26 (dd,  $J$  = 10.8 Hz, 2.4 Hz, 1H), 4.18–4.07 (m, 2H), 3.82 (dd,  $J$  = 11.6 Hz, 4.8 Hz, 1H), 3.14–3.06 (m, 1H), 2.76 (t,  $J$  = 7.2 Hz, 4H), 2.64 (t,  $J$  = 7.2 Hz, 4H), 2.33 (s, 3H), 1.97–1.86 (m, 5H). MS:  $m/z$  432.1 (M +  $\text{H}^+$ ).

(*R*)-*N*-((1,2,3,5,6,7-Hexahydro-s-indacen-4-yl)carbamoyl)-6-(methylamino)-6,7-dihydro-5H-pyrazolo[5,1-*b*][1,3]oxazine-3-sulfonamide sodium salt (**Ent-20**) was prepared in an analogous manner to (*S*)-*N*-((1,2,3,5,6,7-hexahydro-s-indacen-4-yl)carbamoyl)-6-(methylamino)-6,7-dihydro-5H-pyrazolo[5,1-*b*][1,3]oxazine-3-sulfonamide sodium salt (**20**) by replacing (*S*)-methyl 2-((*tert*-butoxycarbonyl)amino)-3-hydroxypropanoate with (*R*)-methyl 2-((*tert*-butoxycarbonyl)amino)-3-hydroxypropanoate.  $^1\text{H}$  NMR (400 MHz, DMSO- $d_6$ )  $\delta$  7.35 (s, 1H), 7.30 (s, 1H), 6.75 (s, 1H), 4.27–4.21 (m, 1H), 4.17–4.12 (m, 1H), 4.08–4.05 (m, 1H), 3.84–3.77 (m, 1H), 3.11–3.03 (m, 1H), 2.76 (t,  $J$  = 8.0 Hz, 4H), 2.65 (t,  $J$  = 7.6 Hz, 4H), 2.33–2.27 (m, 3H), 1.97–1.83 (m, 4H). MS:  $m/z$  432.1 (M +  $\text{H}^+$ ).

(*S*)-6-(Dimethylamino)-*N*-((1,2,3,5,6,7-hexahydro-s-indacen-4-yl)carbamoyl)-6,7-dihydro-5H-pyrazolo[5,1-*b*][1,3]oxazine-3-sulfonamide (**21**). To a solution of 2-aminopropane-1,3-diol (10.0 g, 100 mmol) in ethanol (100 mL) was added di-*tert*-butyl dicarbonate (24.0 g, 100 mmol) at room temperature. After 16 h, the reaction mixture was concentrated under reduced pressure to give *tert*-butyl (1,3-dihydroxypropan-2-yl)carbamate (21.0 g, yield: 100%) as a white solid.

To a solution of *tert*-butyl (1,3-dihydroxypropan-2-yl)carbamate (21.0 g, 100 mmol) and triethylamine (23.0 g, 200 mmol) in  $\text{CH}_2\text{Cl}_2$  (200 mL) was added  $\text{MsCl}$  (26.0 g, 200 mmol) at 0 °C. The reaction mixture was warmed to room temperature. After 2 h, the reaction mixture was filtered, and the filtrate was concentrated to under

reduced pressure to give 2-((*tert*-butoxycarbonyl)amino)propane-1,3-diyi dimethanesulfonate (37.0 g, yield: 97%) as a white solid.

2-((*tert*-butoxycarbonyl)amino)propane-1,3-diyi dimethanesulfonate (37.3 g, 110 mmol), 1*H*-pyrazol-3(2*H*)-one (9.0 g, 0.11 mol), and  $\text{K}_2\text{CO}_3$  (30.0 g, 0.22 mol) in DMF (300 mL) were heated at 120 °C. After 16 h, the reaction mixture was concentrated under reduced pressure. The crude residue was partitioned between ethyl acetate (300 mL) and water (500 mL). The aqueous layer was extracted with ethyl acetate (300 mL). The combined organic layers were washed with brine (100 mL), dried over  $\text{Na}_2\text{SO}_4$ , and concentrated in vacuo to give *rac*-*tert*-butyl (6,7-dihydro-5H-pyrazolo[5,1-*b*][1,3]oxazin-6-yl)carbamate (8.8 g, yield: 34%) as a yellow solid. MS:  $m/z$  240.0 (M +  $\text{H}^+$ ).

NBS (6.5 g, 37.0 mmol) was added portion-wise to a solution of *rac*-*tert*-butyl (6,7-dihydro-5H-pyrazolo[5,1-*b*][1,3]oxazin-6-yl)carbamate (8.8 g, 37.0 mmol) in MeCN (100 mL) at 0 °C. The reaction mixture was warmed to room temperature. After 2 h, the reaction mixture was concentrated, and the crude residue was purified by silica gel column chromatography (petroleum ether/ethyl acetate = 5/1) to give *rac*-*tert*-butyl (3-bromo-6,7-dihydro-5H-pyrazolo[5,1-*b*][1,3]oxazin-6-yl)carbamate (2.5 g, yield: 21%) as a yellow solid. MS:  $m/z$  319.9 (M +  $\text{H}^+$ ).

To a solution of *rac*-*tert*-butyl (3-bromo-6,7-dihydro-5H-pyrazolo[5,1-*b*][1,3]oxazin-6-yl)carbamate (1.0 g, 3.2 mmol) in DCM (5 mL) was added TFA (5 mL) at room temperature. After 20 min, the reaction mixture was concentrated under reduced pressure to give *rac*-3-bromo-6,7-dihydro-5H-pyrazolo[5,1-*b*][1,3]oxazin-6-amine as a yellow solid. MS:  $m/z$  218.0 (M +  $\text{H}^+$ ).

To a solution of *rac*-3-bromo-6,7-dihydro-5H-pyrazolo[5,1-*b*][1,3]oxazin-6-amine (crude, ~3.2 mmol) in MeOH (10 mL) was added HCHO (30%, 3.2 g, 31.5 mmol) at room temperature. After 2 h,  $\text{NaBH}_3\text{CN}$  (2.0 g, 31.5 mmol) was then added, and the reaction mixture was allowed to stir for an additional 16 h at this temperature. The was directly purified by reverse-phase HPLC (0% - 95% MeCN in  $\text{H}_2\text{O}$ ) to give *rac*-3-bromo-*N,N*-dimethyl-6,7-dihydro-5H-pyrazolo[5,1-*b*][1,3]oxazin-6-amine (410 mg, yield: 53%) as a white solid.  $^1\text{H}$  NMR (300 MHz,  $\text{CDCl}_3$ )  $\delta$  7.33 (s, 1H), 4.45–4.44 (m, 1H), 4.30–4.24 (m, 2H), 4.18–4.11 (m, 1H), 3.00–2.97 (m, 1H), 2.40 (s, 6H). MS:  $m/z$  245.9 (M +  $\text{H}^+$ ).

*n*-BuLi (2.5 M in hexane, 0.7 mL, 1.6 mmol) was added to a solution of *rac*-3-bromo-*N,N*-dimethyl-6,7-dihydro-5H-pyrazolo[5,1-*b*][1,3]oxazin-6-amine (400 mg, 1.6 mmol) in THF (5 mL) at -78 °C under nitrogen. After 20 min,  $\text{ZnCl}_2$  (1 M in ether, 1.6 mL, 1.6 mmol) was added. The cooling bath was removed, and the reaction mixture was allowed to warm to room temperature. After 1 h, TCPC (479 mg, 1.6 mmol) was added, and the mixture was stirred at room temperature for an additional 1 h. The rection mixture was diluted with water (30 mL) and ethyl acetate (30 mL). The organic layer was washed with brine (30 mL), dried over  $\text{Na}_2\text{SO}_4$ , and concentrated under reduced pressure to give crude *rac*-2,4,6-trichlorophenyl 6-(dimethylamino)-6,7-dihydro-5H-pyrazolo[5,1-*b*][1,3]oxazine-3-sulfonate as a yellow gel which was used for the next step without purification.

A mixture of *rac*-2,4,6-trichlorophenyl 6-(dimethylamino)-6,7-dihydro-5H-pyrazolo[5,1-*b*][1,3]oxazine-3-sulfonate (crude, ~1.6 mmol),  $\text{NH}_4\text{OH}$  (10 mL), and THF (10 mL) was stirred at 60 °C overnight. The reaction mixture was concentrated under reduced pressure until 10 mL of liquid remained. The remaining solution was acidified with 1 N HCl to pH = 5. The residue was purified by reverse-phase HPLC (0–95% MeCN in  $\text{H}_2\text{O}$ ) to give *rac*-6-(dimethylamino)-6,7-dihydro-5H-pyrazolo[5,1-*b*][1,3]oxazine-3-sulfonamide (66 mg, yield: 16% over two steps) as a white solid.

*rac*-6-(Dimethylamino)-6,7-dihydro-5H-pyrazolo[5,1-*b*][1,3]oxazine-3-sulfonamide (110 mg, 0.4 mmol) was resolved by chiral prep-HPLC to afford (*S*)-6-(dimethylamino)-6,7-dihydro-5H-pyrazolo[5,1-*b*][1,3]oxazine-3-sulfonamide (41 mg, yield: 42%) as a white solid and (*R*)-6-(dimethylamino)-6,7-dihydro-5H-pyrazolo[5,1-*b*][1,3]oxazine-3-sulfonamide (36 mg, yield: 37%) as a white solid.  $^1\text{H}$  NMR (400 MHz, DMSO- $d_6$ )  $\delta$  7.47 (s, 1H), 7.13 (brs, 2H), 4.95–4.41 (m, 2H), 4.23–4.13 (m, 2H), 2.89–2.86 (m, 1H), 2.26 (s, 6H).

NaOMe (12 mg, 0.22 mmol) was added to a solution of (*S*)-6-(dimethylamino)-6,7-dihydro-5H-pyrazolo[5,1-*b*][1,3]oxazine-3-sulfonamide (55 mg, 0.22 mmol) in THF (5 mL) at room temperature. After 20 min, 4-isocyanato-1,2,3,5,6,7-hexahydro-s-indacene (44 mg, 0.22 mmol) was added, and the reaction mixture was allowed to stir for an additional 20 min. The reaction mixture was diluted with water (20 mL) and ethyl acetate (20 mL). The aqueous layer was separated and acidified to pH = 5 with 1 N HCl. The precipitate was collected by filtration and dried to give (*S*)-6-(dimethylamino)-N-((1,2,3,5,6,7-hexahydro-s-indacen-4-yl)carbamoyl)-6,7-dihydro-5H-pyrazolo[5,1-*b*][1,3]oxazine-3-sulfonamide (14 mg, yield: 18%) as a white solid. <sup>1</sup>H NMR (400 MHz, DMSO-d<sub>6</sub>) δ 10.47 (brs, 1H), 7.84 (s, 1H), 7.57 (s, 1H), 6.90 (s, 1H), 4.46–4.43 (m, 2H), 4.24–4.12 (m, 2H), 2.92–2.91 (m, 1H), 2.80 (t, *J* = 7.2 Hz, 4H), 2.64 (t, *J* = 7.2 Hz, 4H), 2.25 (s, 6H), 1.93–1.90 (m, 4H). MS: *m/z* 446.0 (M + H<sup>+</sup>).

(*S*)-*N*-((1,2,3,5,6,7-Hexahydro-s-indacen-4-yl)carbamoyl)-6-(3-methoxyazetidin-1-yl)-6,7-dihydro-5H-pyrazolo[5,1-*b*][1,3]oxazine-3-sulfonamide (**22**). To a solution of 1,3-dibromo-propan-2-ol (42.5 g, 190 mmol) and DHP (33 g, 380 mmol) in DCM (300 mL) was added TsOH (3.6 g, 0.019 mol) at room temperature. After 2 h, the reaction mixture was concentrated under reduced pressure, and the crude residue was purified by silica gel column chromatography (petroleum ether/ethyl acetate = 50/1) to give 2-(2-bromo-1-bromomethyl-ethoxy)-tetrahydro-pyran (34 g, yield: 60%) as a colorless oil. <sup>1</sup>H NMR (300 MHz, DMSO-d<sub>6</sub>) δ 4.80–4.79 (m, 1H), 4.04–3.90 (m, 2H), 3.72–3.52 (m, 5H), 1.87–1.55 (m, 6H).

A mixture of 2-(2-bromo-1-bromomethyl-ethoxy)-tetrahydro-pyran (17 g, 56.3 mmol), 1,2-dihydro-pyrazol-3-one (4 g, 47 mmol), and K<sub>2</sub>CO<sub>3</sub> (23 g, 165 mmol) in DMF (250 mL) was stirred at 100 °C. After 12 h, the reaction mixture was concentrated under reduced pressure. The crude residue was partitioned between ethyl acetate (200 mL) and water (200 mL). The aqueous layer was extracted with ethyl acetate (200 mL). The combined organic layers were washed with water (100 mL) and brine (100 mL), dried over Na<sub>2</sub>SO<sub>4</sub>, and concentrated under reduced pressure. The crude residue was purified by silica gel column chromatography (ethyl acetate) to give 6-(tetrahydro-pyran-2-yloxy)-6,7-dihydro-5H-pyrazolo[5,1-*b*][1,3]oxazine (4.9 g, yield: 46%) as a yellow oil. <sup>1</sup>H NMR (300 MHz, DMSO-d<sub>6</sub>) δ 7.34 (s, 1H), 5.51 (s, 1H), 4.89–4.83 (m, 1H), 4.36–4.24 (m, 4H), 3.93–3.88 (m, 1H), 3.59–3.54 (m, 1H), 1.79–1.69 (m, 3H), 1.65–1.51 (m, 4H). MS: *m/z* 224.9 (M + H<sup>+</sup>).

To a solution of 6-(tetrahydro-pyran-2-yloxy)-6,7-dihydro-5H-pyrazolo[5,1-*b*][1,3]oxazine (5.1 g, 22.8 mmol) in MeCN was added NBS portion-wise at 0 °C. The reaction mixture was warmed to room temperature. After 1 h, the reaction mixture was partitioned between ethyl acetate (100 mL) and water (200 mL). The organic layer was washed with water (100 mL) and brine (100 mL), dried over Na<sub>2</sub>SO<sub>4</sub>, and concentrated under reduced pressure. The crude residue was purified by silica gel column chromatography (petroleum ether/ethyl acetate = 1/1) to give 3-bromo-6-(tetrahydro-pyran-2-yloxy)-6,7-dihydro-5H-pyrazolo[5,1-*b*][1,3]oxazine (5.6 g, yield: 81%) as a yellow solid. <sup>1</sup>H NMR (300 MHz, DMSO-d<sub>6</sub>) δ 7.33 (s, 1H), 4.88–4.82 (m, 1H), 4.48–4.18 (m, 5H), 3.88–3.75 (m, 1H), 3.58–3.53 (m, 1H), 1.84–1.51 (m, 7H). MS: *m/z* 303.0 (M + H<sup>+</sup>).

*n*-BuLi (2.5 M in hexane, 2.6 mL, 6.6 mmol) was added to a solution of 3-bromo-6-(tetrahydro-pyran-2-yloxy)-6,7-dihydro-5H-pyrazolo[5,1-*b*][1,3]oxazine (2 g, 6.6 mmol) in dry THF (20 mL) at -78 °C. After 20 min, ZnCl<sub>2</sub> (1 M in diethyl ether, 6.6 mL, 6.6 mmol) was added, and the reaction mixture was warmed to room temperature. After 1 h, TCPC (2 g, 6.6 mmol) was added, and the mixture was allowed to stir at room temperature for an additional 1 h. The reaction mixture was partitioned between water (100 mL) and ethyl acetate (100 mL). The organic layer was washed with brine (100 mL), dried over Na<sub>2</sub>SO<sub>4</sub>, and concentrated under reduced pressure to give 6-(tetrahydro-pyran-2-yloxy)-6,7-dihydro-5H-pyrazolo[5,1-*b*][1,3]oxazine-3-sulfonic acid 2,4,6-trichloro-phenyl ester, as a yellow gel, which was used in the next step without further purification.

A mixture of 6-(tetrahydro-pyran-2-yloxy)-6,7-dihydro-5H-pyrazolo[5,1-*b*][1,3]oxazine-3-sulfonic acid 2,4,6-trichloro-phenyl

ester (crude, ~6.6 mmol), dibenzylamine (2.5 g, 12.0 mmol), and THF (20 mL) was stirred at 60 °C. After 12 h, the reaction mixture was cooled to room temperature and concentrated under reduced pressure until 10 mL of liquid remained. 1 N aqueous HCl was added to adjust the pH of the solution to pH = 5. The aqueous solution was extracted with ethyl acetate (100 mL × 5). The combined organic layers were dried over Na<sub>2</sub>SO<sub>4</sub> and concentrated under reduced pressure to give *N,N*-dibenzyl-6-((tetrahydro-2H-pyran-2-yl)oxy)-6,7-dihydro-5H-pyrazolo[5,1-*b*][1,3]oxazine-3-sulfonamide (1.5 g, yield: 51%) as a yellow solid. MS: *m/z* 484.2 (M + H<sup>+</sup>).

Concentrated HCl (10 mL) was added to a solution of *N,N*-dibenzyl-6-((tetrahydro-2H-pyran-2-yl)oxy)-6,7-dihydro-5H-pyrazolo[5,1-*b*][1,3]oxazine-3-sulfonamide (6.1 g, 12.6 mmol) in THF/H<sub>2</sub>O/EtOH (50 mL/10 mL/50 mL) at room temperature. After 12 h, the reaction mixture was concentrated under reduced pressure, and the crude residue was purified by reverse-phase HPLC (MeCN/H<sub>2</sub>O) to give *N,N*-dibenzyl-6-hydroxy-6,7-dihydro-5H-pyrazolo[5,1-*b*][1,3]oxazine-3-sulfonamide (4.0 g, yield: 80%) as a white solid. MS: *m/z* 400.1 (M + H<sup>+</sup>).

Dess-Martin periodinane (7.2 g, 17.0 mmol) was added to a solution of *N,N*-dibenzyl-6-hydroxy-6,7-dihydro-5H-pyrazolo[5,1-*b*][1,3]oxazine-3-sulfonamide (3.4 g, 8.5 mmol) in CH<sub>2</sub>Cl<sub>2</sub> (50.0 mL) at room temperature. After 16 h, the mixture was concentrated under reduced pressure, and the crude residue was purified by silica gel column chromatography (petroleum ether/ethyl acetate = 1/2) to give *N,N*-dibenzyl-6-oxo-6,7-dihydro-5H-pyrazolo[5,1-*b*][1,3]oxazine-3-sulfonamide (3.0 g, yield: 91%) as a yellow solid.

Sodium triacetoxyborohydride (848 mg, 4.0 mmol) was added to a solution of *N,N*-dibenzyl-6-oxo-6,7-dihydro-5H-pyrazolo[5,1-*b*][1,3]oxazine-3-sulfonamide (794 mg, 2.0 mmol) and azetidin-3-ol hydrochloride (440 mg, 4.0 mmol) in MeOH (30 mL) at room temperature. After 30 min, sodium cyanoborohydride (252 mg, 4.0 mmol) was added, and the reaction mixture was allowed to stir at this temperature for an additional 16 h. The reaction mixture was concentrated in vacuo, and the crude residue was purified by silica gel column chromatography (CH<sub>2</sub>Cl<sub>2</sub>/MeOH = 5/1) to give *rac*-*N,N*-dibenzyl-6-(3-hydroxyazetidin-1-yl)-6,7-dihydro-5H-pyrazolo[5,1-*b*][1,3]oxazine-3-sulfonamide (340 mg, yield: 37%) as a yellow solid. MS: *m/z* 455.2 (M + H<sup>+</sup>).

To a solution of *rac*-*N,N*-dibenzyl-6-(3-hydroxyazetidin-1-yl)-6,7-dihydro-5H-pyrazolo[5,1-*b*][1,3]oxazine-3-sulfonamide (105 mg, 0.2 mmol) in DMF (3 mL) was added NaH (60% in mineral oil, 14.0 mg, 0.4 mmol) at room temperature. After 1 h, iodomethane (39.0 mg, 0.3 mmol) was added, and the mixture was allowed to stir at room temperature for an additional 2 h. The reaction mixture was poured into water (20 mL), and the aqueous layer was extracted with ethyl acetate (20 mL). The organic layer was washed with water (10 mL) and brine (10 mL), dried over Na<sub>2</sub>SO<sub>4</sub>, and concentrated under reduced pressure to give *rac*-*N,N*-dibenzyl-6-(3-methoxyazetidin-1-yl)-6,7-dihydro-5H-pyrazolo[5,1-*b*][1,3]oxazine-3-sulfonamide (120 mg, crude) as a yellow oil. MS: *m/z* 469.1 (M + H<sup>+</sup>).

Concentrated H<sub>2</sub>SO<sub>4</sub> (0.32 mL) was added to a solution of *rac*-*N,N*-dibenzyl-6-(3-methoxyazetidin-1-yl)-6,7-dihydro-5H-pyrazolo[5,1-*b*][1,3]oxazine-3-sulfonamide (120 mg, 0.3 mmol) in CH<sub>2</sub>Cl<sub>2</sub> (3.0 mL) at room temperature. After 30 min, the reaction mixture was concentrated under reduced pressure. Saturated aqueous NaHCO<sub>3</sub> was added to the residue. The mixture was filtered, and the filtrate was purified by reverse-phase HPLC (MeCN/H<sub>2</sub>O) to give *rac*-6-(3-methoxyazetidin-1-yl)-6,7-dihydro-5H-pyrazolo[5,1-*b*][1,3]oxazine-3-sulfonamide (52.0 mg, yield: 70%) as a white solid. MS: *m/z* 289.1 (M + H<sup>+</sup>).

*rac*-6-(3-Methoxyazetidin-1-yl)-6,7-dihydro-5H-pyrazolo[5,1-*b*][1,3]oxazine-3-sulfonamide (150 mg) was resolved by chiral prep-HPLC to give (*R*)-6-(3-methoxyazetidin-1-yl)-6,7-dihydro-5H-pyrazolo[5,1-*b*][1,3]oxazine-3-sulfonamide (65 mg) as a white solid (*S*)-6-(3-methoxyazetidin-1-yl)-6,7-dihydro-5H-pyrazolo[5,1-*b*][1,3]oxazine-3-sulfonamide (60 mg) as a white solid.

(*S*)-((1,2,3,5,6,7-Hexahydro-s-indacen-4-yl)carbamoyl)((6-(3-methoxyazetidin-1-yl)-6,7-dihydro-5H-pyrazolo[5,1-*b*][1,3]oxazine-3-yl)sulfonyl)amide was prepared in a similar manner to (*S*)-6-

(dimethylamino)-*N*-((1,2,3,5,6,7-hexahydro-*s*-indacen-4-yl)-carbamoyl)-6,7-dihydro-5*H*-pyrazolo[5,1-*b*][1,3]oxazine-3-sulfonamide specifically by replacing (*S*)-6-(dimethylamino)-6,7-dihydro-5*H*-pyrazolo[5,1-*b*][1,3]oxazine-3-sulfonamide with (*S*)-6-(3-methoxyazetidin-1-yl)-6,7-dihydro-5*H*-pyrazolo[5,1-*b*][1,3]oxazine-3-sulfonamide. <sup>1</sup>H NMR (400 MHz, DMSO-*d*<sub>6</sub>)  $\delta$  7.39 (brs, 1H), 7.30 (s, 1H), 6.76 (s, 1H), 4.12–4.06 (m, 3H), 3.95–3.92 (m, 1H), 3.79–3.76 (m, 1H), 3.55–3.52 (m, 2H), 3.14 (s, 3H), 2.98–2.92 (m, 2H), 2.88 (br, 1H), 2.75 (t, *J* = 7.2 Hz, 4H), 2.66 (t, *J* = 7.2 Hz, 4H), 1.95–1.87 (m, 4H). MS: *m/z* 488.2 (M + H<sup>+</sup>).

**6-((Dimethylamino)methyl)-*N*-((1,2,3,5,6,7-hexahydro-*s*-indacen-4-yl)carbamoyl)-6,7-dihydro-5*H*-pyrazolo[5,1-*b*][1,3]oxazine-3-sulfonamide (23).** A mixture of 1,2-dihydro-pyrazol-3-one (10.4 g, 124 mmol) and K<sub>2</sub>CO<sub>3</sub> (42.8 g, 310 mmol) in DMF (700 mL) was heated to 100 °C. 3-Chloro-2-chloromethyl-propene (15.5 g, 124 mmol) was added, and the mixture was stirred at 100 °C for 16 hrs. The solvent was removed in vacuo. The crude residue was partitioned between ethyl acetate (200 mL) and water (500 mL). The aqueous layer was extracted with ethyl acetate (200 mL). The combined organic layers were washed with brine (100 mL), dried over Na<sub>2</sub>SO<sub>4</sub>, and concentrated under reduced pressure. The crude residue was purified by silica gel column chromatography (petroleum ether/ethyl acetate = 1/1) to give 6-methylene-6,7-dihydro-5*H*-pyrazolo[5,1-*b*][1,3]oxazine (1.7 g, yield: 10%) as a yellow oil. <sup>1</sup>H NMR (300 MHz, CDCl<sub>3</sub>)  $\delta$  7.34 (s, 1H), 5.51 (s, 1H), 5.39 (s, 2H), 4.80 (s, 2H), 4.63 (s, 2H). MS: *m/z* 137.1 (M + H<sup>+</sup>).

To a solution of 6-methylene-6,7-dihydro-5*H*-pyrazolo[5,1-*b*][1,3]-oxazine (1.7 g, 12.5 mmol) in THF (20 mL) was added BH<sub>3</sub>/Me<sub>2</sub>S (10 M, 5 mL, 50 mmol) at 0 °C. The reaction mixture was warmed to room temperature and was allowed to stir at this temperature for 16 h. Then, 3 M aqueous NaOH (50 mL, 150 mmol) and H<sub>2</sub>O<sub>2</sub> (30%, 5.7 g, 50 mmol) were added to the reaction mixture slowly. The reaction mixture was heated to 80 °C. After 2 h, the reaction mixture was cooled to room temperature, and saturated aqueous Na<sub>2</sub>SO<sub>3</sub> (50 mL) was added. The reaction mixture was allowed to stir at room temperature for 30 min. Then the resulting mixture was extracted with ethyl acetate (100 mL × 3). The combined organic layers were washed with brine (100 mL), dried over Na<sub>2</sub>SO<sub>4</sub>, and concentrated under reduced pressure to give (6,7-dihydro-5*H*-pyrazolo[5,1-*b*][1,3]oxazin-6-yl)-methanol (1.3 g, yield: 68%) as a yellow oil. <sup>1</sup>H NMR (300 MHz, CDCl<sub>3</sub>)  $\delta$  7.31 (d, *J* = 1.8 Hz, 1H), 5.49 (d, *J* = 1.8 Hz, 1H), 4.37 (dd, *J* = 11.4, 3 Hz, 1H), 4.28–4.12 (m, 2H), 4.07–4.00 (m, 1H), 3.77 (d, *J* = 6.6 Hz, 2H), 2.58–2.50 (m, 1H).

To a solution of (6,7-dihydro-5*H*-pyrazolo[5,1-*b*][1,3]oxazin-6-yl)-methanol (2.05 g, 13.3 mmol) in THF (30 mL) were added DPPA (7.3 g, 26.6 mmol) and DBU (6.1 g, 39.9 mmol) at room temperature. The suspension was heated to 60 °C. After 16 h, the reaction mixture was diluted with ethyl acetate (100 mL) and water (100 mL). The organic layer was separated. The aqueous layer was extracted with ethyl acetate (100 mL). The combined organic layers were washed with brine (100 mL), dried over Na<sub>2</sub>SO<sub>4</sub>, and concentrated in vacuo. The crude residue was purified by silica gel column chromatography (petroleum ether/ethyl acetate = 2/1) to give 6-azidomethyl-6,7-dihydro-5*H*-pyrazolo[5,1-*b*][1,3]oxazine (1.24 g, yield: 62%) as a yellow oil. MS: *m/z* 180.3 (M + H<sup>+</sup>).

To a solution of 6-azidomethyl-6,7-dihydro-5*H*-pyrazolo[5,1-*b*][1,3]oxazine (1.24 g, 16.9 mmol) in MeOH (20 mL) were added Boc<sub>2</sub>O (3 g, 13.8 mmol) and Pd/C (5%, 0.2 g) at room temperature, and the mixture was stirred under a H<sub>2</sub> atmosphere. After 16 h, the reaction mixture was filtered, and the filtrate was concentrated to give *tert*-butyl ((6,7-dihydro-5*H*-pyrazolo[5,1-*b*][1,3]oxazin-6-yl)methyl)-carbamate, which was used in the next step without further purification. MS: *m/z* 254.0 (M + H<sup>+</sup>).

NBS (1.3 g, 24.7 mmol) was added portion-wise to a solution of *tert*-butyl ((6,7-dihydro-5*H*-pyrazolo[5,1-*b*][1,3]oxazin-6-yl)methyl)-carbamate (crude, 6.9 mmol) in MeCN (20 mL) at 0 °C. The reaction mixture was warmed to room temperature. After 2 h, the mixture was filtered, and the filtrate was purified by reverse-phase HPLC (5% – 95% MeCN in H<sub>2</sub>O) to give *tert*-butyl ((3-bromo-6,7-

dihydro-5*H*-pyrazolo[5,1-*b*][1,3]oxazin-6-yl)methyl)carbamate (1.62 g, yield: 71%) as a yellow solid. MS: *m/z* 331.9 (M + H<sup>+</sup>).

2,4,6-Trichlorophenyl 6-(((*tert*-butoxycarbonyl)amino)methyl)-6,7-dihydro-5*H*-pyrazolo[5,1-*b*][1,3]oxazine-3-sulfonate was prepared in a similar manner to 6-(tetrahydro-pyran-2-yloxy)-6,7-dihydro-5*H*-pyrazolo[5,1-*b*][1,3]oxazine-3-sulfonic acid 2,4,6-trichloro-phenyl ester.

*rac*-*tert*-butyl ((3-sulfamoyl-6,7-dihydro-5*H*-pyrazolo[5,1-*b*][1,3]-oxazin-6-yl)methyl)carbamate was prepared in a similar manner to *rac*-6-(dimethylamino)-6,7-dihydro-5*H*-pyrazolo[5,1-*b*][1,3]oxazine-3-sulfonamide. MS: *m/z* 333.4 (M + H<sup>+</sup>).

HCl/dioxane (4 M, 1 mL, 4 mmol) was added to a solution of *rac*-*tert*-butyl ((3-sulfamoyl-6,7-dihydro-5*H*-pyrazolo[5,1-*b*][1,3]oxazin-6-yl)methyl)carbamate (110 mg, 0.33 mmol) in MeOH (2 mL) at 0 °C. The reaction mixture was warmed to room temperature. After 2 h, the reaction mixture was concentrated under reduced pressure to give *rac*-6-(aminomethyl)-6,7-dihydro-5*H*-pyrazolo[5,1-*b*][1,3]oxazine-3-sulfonamide hydrochloride, which was used directly in the next step without further purification.

To a solution of *rac*-6-(aminomethyl)-6,7-dihydro-5*H*-pyrazolo[5,1-*b*][1,3]oxazine-3-sulfonamide hydrochloride (crude, 0.33 mmol) in MeOH (2 mL) was added HCHO (1.5 mL) followed by NaCNBH<sub>3</sub> (20.8 mg, 0.33 mmol) at room temperature. After 3 h, the reaction mixture was filtered, and the filtrate was purified by reverse-phase HPLC (MeCN/H<sub>2</sub>O) to give *rac*-6-((dimethylamino)methyl)-6,7-dihydro-5*H*-pyrazolo[5,1-*b*][1,3]oxazine-3-sulfonamide (50 mg, yield: 59%) as a white solid. MS: *m/z* 261.1 (M + H<sup>+</sup>).

*rac*-6-((Dimethylamino)methyl)-*N*-((1,2,3,5,6,7-hexahydro-*s*-indacen-4-yl)carbamoyl)-6,7-dihydro-5*H*-pyrazolo[5,1-*b*][1,3]oxazine-3-sulfonamide was prepared in a similar manner to (S)-((1,2,3,5,6,7-hexahydro-*s*-indacen-4-yl)carbamoyl)((6-(3-methoxyazetidin-1-yl)-6,7-dihydro-5*H*-pyrazolo[5,1-*b*][1,3]oxazin-3-yl)sulfonyl)amide specifically by replacing (S)-6-(3-methoxyazetidin-1-yl)-6,7-dihydro-5*H*-pyrazolo[5,1-*b*][1,3]oxazin-3-sulfonamide with *rac*-6-((dimethylamino)methyl)-6,7-dihydro-5*H*-pyrazolo[5,1-*b*][1,3]oxazine-3-sulfonamide. <sup>1</sup>H NMR (400 MHz, DMSO-*d*<sub>6</sub>, CD<sub>3</sub>OD)  $\delta$  7.37 (s, 1H), 7.32 (s, 1H), 6.75 (s, 1H), 4.37 (dd, *J* = 6.8, 2.8 Hz, 1H), 4.10–4.00 (m, 2H), 3.80–3.75 (m, 1H), 2.74 (t, *J* = 7.2 Hz, 4H), 2.64 (t, *J* = 7.2 Hz, 4H), 2.47–2.43 (m, 1H), 2.23 (d, *J* = 7.2 Hz, 2H), 2.14 (s, 6H), 1.95–1.85 (m, 4H). MS: *m/z* 460.1 (M + H<sup>+</sup>).

**Measurement of IL-1 $\beta$  and TNF $\alpha$  in LPS + Nigericin Stimulated PBMCs.** hPBMCs consisting of lymphocytes (T, B, and NK cells), monocytes, and dendritic cells were freshly isolated from human peripheral blood from healthy donors. Cells were obtained through an IRB-approved donor program by iXCells Biotechnologies where all the donors were tested for bacterial and viral infections. Cells were purified from peripheral blood using Ficoll gradient centrifugation.

Fresh or cryopreserved PMBCs were seeded in V-bottom 96-well plates at 0.5–1 × 10<sup>5</sup> cells per well and incubated overnight at 37 °C with 5% CO<sub>2</sub> in RPMI 1640 medium with GlutaMAX supplement, 4.5 g/L d-glucose, 10% fetal bovine serum (FBS), 100 mM sodium pyruvate, 1% penicillin/streptomycin, 10 mM HEPES, and 0.05 mM  $\beta$ -mercaptoethanol. Cryopreserved Kupffer cells were thawed and seeded in flat-bottom 96-well plates at 0.6–1.5 × 10<sup>5</sup> cells/well and incubated overnight at 37 °C, 5% CO<sub>2</sub> in RPMI 1640 Medium with GlutaMAX supplement, FBS, 1% penicillin/streptomycin, and 10 mM HEPES. The following day, the cells were primed with 100 ng/mL of lipopolysaccharides (LPS; Sigma-Aldrich) in FBS-free RPMI 1640 for 3 h. After the priming step, the media were removed, and PBMCs were preincubated with serial concentrations of test compounds (0.00017–10  $\mu$ M) or vehicle (DMSO) for 30 min in FBS-free media prior to addition of the NLRP3 activator. Cells were then stimulated with 10  $\mu$ M nigericin (InvivoGen; trl-nig-5) for 1.5 h. Plates were centrifuged at 1500 rpm for 3 min to pellet cells, and the supernatant was transferred into new plates for subsequent experiments. For ELISA assays, cells were seeded into 96-well plates. Levels of mature IL-1 $\beta$  and TNF $\alpha$  in cell-conditioned media were measured by ELISA (Quantikine ELISA, R&D systems) according to the manufacturer's

instructions. Pyroptosis was measured using cell titer glo reagent (Promega) according to the manufacturer's instructions.

**THP-1 ASC-GFP Speck Assay.** The THP-1 ASC-GFP cell line was purchased from Invivogen, San Diego, for inflammasome activation assay. THP-1 ASC-GFP cells stably express a 37.6 kDa ASC::GFP fusion protein that enables monitoring of speck formation by fluorescence microscopy after activation of the NLRP3-dependent inflammasome pathway. Cells were maintained at a density of 600,000 cells/mL in growth media consisting of RPMI 1640, 2 mM L-glutamine, 25 mM HEPES, and 10% heat-inactivated FBS at 37 °C and 5% CO<sub>2</sub>. Cells were passaged every 3–4 days and used for assays for up to 20 passages.

THP-1 ASC-GFP cells were collected by centrifuging cells at 800 RPM for 5 min. The cell culture supernatant was removed, and cells were re-suspended in fresh media at a density of  $1 \times 10^6$  cells/mL in assay media consisting of RPMI 1640, 2 mM L-glutamine, 25 mM HEPES, and 10% heat-inactivated FBS. Phorbol 12-myristate 13-acetate (PMA) (Invivogen, trl-pma) was added to the cell suspension at a final concentration of 500 ng/mL and mixed thoroughly. Subsequently,  $4 \times 10^4$  cells/well were seeded in a 384-well plate and differentiated into macrophages overnight at 37 °C and 5% CO<sub>2</sub>. Cells were primed with 1 µg/mL of LPS (Invivogen Ultrapure lipopolysaccharide from *Escherichia coli*, trl-3pelps) in assay media for 3 h at 37 °C and 5% CO<sub>2</sub>. After priming, media were removed, and THP-1 ASC-GFP cells were preincubated with serially diluted test compounds with a starting concentration of 40 µM followed by 2-fold dilution for a 20-point curve or vehicle (DMSO) for 30 min in assay media at 37 °C and 5% CO<sub>2</sub>. Cells were then stimulated with 10 µM nigericin (Invivogen, trl-nig-5) for 90 min at 37 °C and 5% CO<sub>2</sub> to activate the NLRP3-dependent inflammasome pathway and speck formation. After stimulation, cells were fixed with 4.8% paraformaldehyde (Electron Microscopy Sciences #15710-S) and incubated at room temperature for 15 min. Cells were then washed three times with 100 µL of phosphate buffered saline and permeabilized in the presence of permeabilization/block buffer for 20 min at room temperature. After three washes with 100 µL of phosphate buffered saline, cells were incubated for 1 h at room temperature in the presence of Hoechst. After staining with Hoechst, cells were washed three times with 100 µL of phosphate buffered saline and imaged for ASC spec formation. THP-1 ASC-GFP cells were imaged using Alexafluor488 and Hoechst fluorophores. The Hoechst positive signal was used for cell count, and the Alexafluor488 positive signal was used to identify the number of GFP ASC specks in imaged fields. Percentage of cells with a speck was calculated by dividing the number of GFP positive spots by the total number of cells.

**Inflammasome Selectivity Assay in the Human THP-1 Cell Line.** THP-1 and THP-1 NLRC4 cells were collected by centrifuging cells at 1500 RPM for 5 min. The cell culture supernatant was removed, and cells were re-suspended in fresh media at a density of  $1 \times 10^6$  cells/mL in assay media consisting of RPMI 1640, 2 mM L-glutamine, 25 mM HEPES, and 10% heat-inactivated FBS. For NLRP3 activation, THP-1 cells were seeded at  $5 \times 10^4$  cells/well in a 384-well plate. Then, cells were primed with 1 µg/mL of LPS trl-nig-5 (Invivogen Ultrapure lipopolysaccharide from *E. coli*, trl-3pelps) in assay media for 3 h at 37 °C and 5% CO<sub>2</sub>. After priming, THP-1 ASC-GFP cells were incubated with serially diluted GDC-2394 (20) with a starting concentration of 20 µM followed by 3-fold dilution for a 11-point curve or vehicle (DMSO) for 30 min in assay media at 37 °C and 5% CO<sub>2</sub>. Cells were then stimulated with 20 µM nigericin (Invivogen, trl-nig-5) for 90 min at 37 °C and 5% CO<sub>2</sub> to activate NLRP3 dependent inflammasome pathway and caspase-1 activation. For NLRC4 activation,  $5 \times 10^4$  THP-1 NLRC4 cells/well were added in a 384-well plate and incubated with serially diluted GDC-2394 (20) with a starting concentration of 10 µM followed by 3-fold dilution for a 11-point curve or vehicle (DMSO) for 30 min in assay media at 37 °C and 5% CO<sub>2</sub>. Cells were then stimulated with 1 µM Flagellin (Flagellin PA ultrapure, Invivogen: trl-pafla) for 6 h at 37 °C and 5% CO<sub>2</sub> to activate the NLRC4-dependent inflammasome pathway and caspase-1 activation. Caspase-1 activity in cell cultures was measured using a Caspase-Glo 1 assay kit (Promega, G9951)

according to the manufacturer's protocol. An equal volume of Caspase-Glo 1 reagent was added in each well and mixed well followed by 60 min incubation at room temperature. Luminescence was measured using an Envision plate reader.

**Inflammasome Selectivity Assay in Mouse Bone Marrow-Derived Macrophages.** BMDMs were generated by culturing bone marrow cells in the presence of 10 ng/mL of M-CSF for 7 days, with supplementation of fresh media on day 3. On Day 8, BMDMs were stimulated either in the presence of LPS and nigericin to activate the NLRP3 inflammasome pathway or P3CSK4 and flagellin (transfected) to activate the NLRC4 inflammasome pathway.

**Production of Human Monocyte-Derived Macrophages for Inflammasome Activation Assays.** PBMCs were isolated from heparinized blood (Genentech donor program) by Ficoll-paque (Millipore Sigma). CD14<sup>+</sup> primary human monocytes were purified from PBMCs by a Pan Monocyte Isolation Kit (Miltenyi Biotech) according to the manufacturer's instructions and differentiated to macrophages in RPMI with 10% FBS, 10 mM HEPES, and L-glutamine containing M-CSF (PUR59348, Genentech) for 7 days.

**Source and Preparation of Crystals for Inflammasome Activation Assays.** Monosodium urate (trl-msu-25) and calcium pyrophosphate dihydrate (trl-cppd) crystals were obtained from Invivogen. Cholesterol crystals were prepared as described in the literature.<sup>38</sup>

**Measurement of Human IL-1 $\beta$  and IL-18.** Concentrations of human IL-1 $\beta$  and IL-18 in culture supernatants were measured using electrochemiluminescence assays (U-PLEX, Meso Scale Discovery) following the manufacturer's instructions.

**Mouse Acute Peritonitis Challenge Model.** Female C57BL/6 animals were orally gavaged with varying doses of GDC-2394 (20) or vehicle control, and then 2 h later injected intra peritoneally (i.p.) with 1.25 µg LPS followed by 1 mg monosodium urate crystals i.p. a further 2 h later. After 30 min, mice were culled, and peritoneal lavage with PBS was collected for IL-1 $\beta$  assessment using the mouse IL-1 $\beta$ /IL-1F2 DuoSet ELISA (R&D Systems).

**Rat Gouty Arthritis Model.** Baseline knee diameters were measured using a digital caliper, and paw mechanical allodynia was measured by von Frey fibers in male Wistar rats (10 per cohort). Animals were anesthetized 1 day later and injected into the left knee with 2 mg of MSU crystals. 3 h after MSU intra-articular injection, the cohorts were dosed with 25 mg/kg GDC-2394 (20) (oral gavage), 50 mg/kg anakinra (IL-1 receptor antagonist, intra peritoneal), or 0.5 mg/kg colchicine (subcutaneous), and 4 h later, mechanical allodynia responses and knee diameters were recorded. Compound and anakinra dosing was continued once daily for 7 days while colchicine dosing was continued on days 2, 4, and 6, with allodynia and knee swelling assessed 1 h after each round of dosing.

## ASSOCIATED CONTENT

### SI Supporting Information

The Supporting Information is available free of charge at <https://pubs.acs.org/doi/10.1021/acs.jmedchem.2c01250>.

Molecular formula strings ([CSV](#))

In vivo PK study procedures, cross species PK for compound 1, supporting figures and animal information for safety studies, supporting tables for compound 17 and GDC-2394 (20) solubility measurements, molecular formula strings, and cryo-EM data ([PDF](#))

## AUTHOR INFORMATION

### Corresponding Authors

Michael J. Townsend — Genentech Inc., South San Francisco, California 94080, United States;

Email: [townsend.michael@gene.com](mailto:townsend.michael@gene.com)

Craig E. Stivala — Genentech Inc., South San Francisco, California 94080, United States; [orcid.org/0000-0002-5024-6346](https://orcid.org/0000-0002-5024-6346); Email: [stivala.craig@gene.com](mailto:stivala.craig@gene.com)

**Authors**

**Christopher McBride** — Jecure Therapeutics, San Diego, California 92121, United States; Present Address: 858 Therapeutics, San Diego, California 92121, United States  
**Lynn Trzoss** — Jecure Therapeutics, San Diego, California 92121, United States  
**Davide Povero** — Jecure Therapeutics, San Diego, California 92121, United States; Present Address: Mayo Clinic, Rochester, Minnesota 55905, United States  
**Milos Lazic** — Jecure Therapeutics, San Diego, California 92121, United States; Present Address: 858 Therapeutics, San Diego, California 92121, United States  
**Geza Ambrus-Aikelin** — Jecure Therapeutics, San Diego, California 92121, United States; Present Address: Odyssey Therapeutics, San Diego, California 92121, United States  
**Angelina Santini** — Jecure Therapeutics, San Diego, California 92121, United States; Present Address: 858 Therapeutics, San Diego, California 92121, United States  
**Rama Pranadinata** — Jecure Therapeutics, San Diego, California 92121, United States; Present Address: NotumNB INC, Carlsbad, California 92011, United States  
**Gretchen Bain** — Jecure Therapeutics, San Diego, California 92121, United States; Present Address: 858 Therapeutics, San Diego, California 92121, United States; [orcid.org/0000-0001-7513-9486](https://orcid.org/0000-0001-7513-9486)  
**Ryan Stansfield** — Jecure Therapeutics, San Diego, California 92121, United States; Present Address: 858 Therapeutics, San Diego, California 92121, United States  
**Jeffrey A. Stafford** — Jecure Therapeutics, San Diego, California 92121, United States; Present Address: 858 Therapeutics, San Diego, California 92121, United States  
**James Veal** — Jecure Therapeutics, San Diego, California 92121, United States; Present Address: 858 Therapeutics, San Diego, California 92121, United States  
**Ryan Takahashi** — Genentech Inc., South San Francisco, California 94080, United States; Present Address: Denali Therapeutics, South San Francisco, California 94080, United States  
**Justin Ly** — Genentech Inc., South San Francisco, California 94080, United States  
**Shu Chen** — Genentech Inc., South San Francisco, California 94080, United States  
**Liling Liu** — Genentech Inc., South San Francisco, California 94080, United States  
**Marika Nespi** — Genentech Inc., South San Francisco, California 94080, United States  
**Robert Blake** — Genentech Inc., South San Francisco, California 94080, United States  
**Arna Katewa** — Genentech Inc., South San Francisco, California 94080, United States  
**Tracy Kleinheinz** — Genentech Inc., South San Francisco, California 94080, United States  
**Swathi Sujatha-Bhaskar** — Genentech Inc., South San Francisco, California 94080, United States  
**Nandhini Ramamoorthi** — Genentech Inc., South San Francisco, California 94080, United States  
**Jessica Sims** — Genentech Inc., South San Francisco, California 94080, United States  
**Brent McKenzie** — Genentech Inc., South San Francisco, California 94080, United States; Present Address: Sonoma Biotherapeutics, South San Francisco, California 94080, United States.

**Mark Chen** — Genentech Inc., South San Francisco, California 94080, United States  
**Mark Ultsch** — Genentech Inc., South San Francisco, California 94080, United States  
**Matthew Johnson** — Genentech Inc., South San Francisco, California 94080, United States  
**Jeremy Murray** — Genentech Inc., South San Francisco, California 94080, United States; [orcid.org/0000-0002-2161-9326](https://orcid.org/0000-0002-2161-9326)  
**Claudio Ciferri** — Genentech Inc., South San Francisco, California 94080, United States  
**Steven T. Staben** — Genentech Inc., South San Francisco, California 94080, United States; Present Address: Lycia Therapeutics, South San Francisco, California 94080, United States; [orcid.org/0000-0002-6137-6517](https://orcid.org/0000-0002-6137-6517)

Complete contact information is available at:  
<https://pubs.acs.org/10.1021/acs.jmedchem.2c01250>

**Notes**

The authors declare no competing financial interest.

**ACKNOWLEDGMENTS**

We wish to express our gratitude to Shangfeng Li and his team at Sundia Meditech for the synthesis of a number of compounds described herein.

**ABBREVIATIONS**

ATP, adenosine triphosphate; BSEP, bile salt export pump; BUN, blood urea nitrogen; CHC, cholesterol crystals;  $CL_{hep}$ , predictive hepatic clearance;  $CL_p$ , plasma clearance; cLogP, calculated water – octanol partition coefficient; cLogD, calculated water – octanol partition coefficient at pH = 7.4; CPPD, calcium pyrophosphate dihydrate; DILI, drug-induced liver injury; %F, percent fraction absorbed; F, female; gMDCK, Genentech Madin-Darby canine kidney cell line; GSH, glutathione; H/R/M/D/C, human/rat/mouse/dog/cynomolgus monkey; hERG, human *Ether-à-go-go*-related gene; HWB, human whole blood;  $IC_{50}$ , 50% inhibitory concentration;  $IC_{70}$ , 70% inhibitory concentration;  $IC_{90}$ , 90% inhibitory concentration; KC, Kupffer cell; LLE, lipophilic ligand efficiency; LPS, lipopolysaccharide; M, male; MWB, mouse whole blood;  $n$ , number of replicates;  $P_{app}$  (A:B), apparent permeability from the apical to basolateral chamber; PBMCs, peripheral blood mononuclear cell; PPB, plasma protein binding;  $R_t$ , retention time; SD, standard deviation;  $T_{1/2}$ , plasma half-life;  $V_{ss}$ , steady-state volume of distribution; WB, whole blood

**REFERENCES**

- (1) Guo, H.; Callaway, J. B.; Ting, J. P. Y. Inflammasomes: Mechanism of Action, Role in Disease, and Therapeutics. *Nat. Med.* **2015**, *21*, 677–687.
- (2) Dixit, V. M.; Broz, P. Inflammasomes: mechanism of assembly, regulation and signalling. *Nat. Rev. Immunol.* **2016**, *16*, 407–420.
- (3) Taabazuing, C. Y.; Griswold, A. R.; Bachovchin, D. A. The NLRP1 and CARD8 inflammasomes. *Immunol. Rev.* **2020**, *297*, 13–25.
- (4) Kayagaki, N.; Stowe, I. B.; Lee, B. L.; O'Rourke, K.; Anderson, K.; Warming, S.; Cuellar, T.; Haley, B.; Roose-Girma, M.; Phung, Q. T.; Liu, P. S.; Lill, J. R.; Li, H.; Wu, J.; Kummerfeld, S.; Zhang, J.; Lee, W. P.; Snipes, S. J.; Salvesen, G. S.; Morris, L. X.; Fitzgerald, L.; Zhang, Y.; Bertram, E. M.; Goodnow, C. C.; Dixit, V. M. Caspase-11 Cleaves Gasdermin D for Non-Canonical Inflammasome Signaling. *Nature* **2015**, *526*, 666–671.

- (5) Agostini, L.; Martinon, F.; Burns, K.; McDermott, M. F.; Hawkins, P. N.; Tschopp, J. NALP3 Forms an IL-1 $\beta$ -Processing Inflammasome with Increased Activity in Muckle-Wells Autoinflammatory Disorder. *Immunity* **2004**, *20*, 319–325.
- (6) Hoffman, H. M.; Mueller, J. L.; Broide, D. H.; Wanderer, A. A.; Kolodner, R. D. Mutation of a New Gene Encoding a Putative Pyrin-like Protein Causes Familial Cold Autoinflammatory Syndrome and Muckle-Wells Syndrome. *Nat. Genet.* **2001**, *29*, 301–305.
- (7) Mridha, A. R.; Wree, A.; Robertson, A. A. B.; Yeh, M. M.; Johnson, C. D.; van Rooyen, D. M.; Haczeyni, F.; Teoh, N. C. H.; Savard, C.; Ioannou, G. N.; Masters, S. L.; Schroder, K.; Cooper, M. A.; Feldstein, A. E.; Farrell, G. C. NLRP3 Inflammasome Blockade Reduces Liver Inflammation and Fibrosis in Experimental NASH in Mice. *J. Hepatol.* **2017**, *66*, 1037–1046.
- (8) Mangan, M. S. J.; Olhava, E. J.; Roush, W. R.; Seidel, H. M.; Glick, G. D.; Latz, E. Targeting the NLRP3 Inflammasome in Inflammatory Diseases. *Nat. Rev. Drug Discovery* **2018**, *17*, 588–606.
- (9) Swanson, K. v.; Deng, M.; Ting, J. P. Y. The NLRP3 Inflammasome: Molecular Activation and Regulation to Therapeutics. *Nat. Rev. Immunol.* **2019**, *19*, 477–489.
- (10) Zhang, K. E.; Naue, J. A.; Arison, B.; Vyas, K. P. Efficacy and Pharmacology of the NLRP3 Inflammasome Inhibitor CP-456,773 (CRID3) in Murine Models of Dermal and Pulmonary Inflammation. *Nature* **2019**, *21*, 105–121.
- (11) Urban, F. J.; Jasys, V. J. Efficient synthesis of furan sulfonamide compounds useful in the synthesis of new IL-1 inhibitors. US6022984A
- (12) Laliberte, R. E.; Perregaux, D. G.; Hoth, L. R.; Rosner, P. J.; Jordan, C. K.; Peese, K. M.; Eggler, J. F.; Dombroski, M. A.; Geoghegan, K. F.; Gabel, C. A. Glutathione S-Transferase Omega 1-1 Is a Target of Cytokine Release Inhibitory Drugs and May Be Responsible for Their Effect on Interleukin-1 $\beta$  Posttranslational Processing. *J. Biol. Chem.* **2003**, *278*, 16567–16578.
- (13) Coll, R. C.; Robertson, A. A. B.; Chae, J. J.; Higgins, S. C.; Muñoz-Planillo, R.; Inserra, M. C.; Vetter, I.; Dungan, L. S.; Monks, B. G.; Stutz, A.; Croker, D. E.; Butler, M. S.; Haneklaus, M.; Sutton, C. E.; Núñez, G.; Latz, E.; Kastner, D. L.; Mills, K. H. G.; Masters, S. L.; Schroder, K.; Cooper, M. A.; O'Neill, L. A. J. A Small-Molecule Inhibitor of the NLRP3 Inflammasome for the Treatment of Inflammatory Diseases. *Nat. Med.* **2015**, *21*, 248–255.
- (14) Primiano, M. J.; Lefker, B. A.; Bowman, M. R.; Bree, A. G.; Hubeau, C.; Bonin, P. D.; Mangan, M.; Dower, K.; Monks, B. G.; Cushing, L.; Wang, S.; Guzova, J.; Jiao, A.; Lin, L.-L.; Latz, E.; Hepworth, D.; Hall, J. P. Efficacy and Pharmacology of the NLRP3 Inflammasome Inhibitor CP-456,773 (CRID3) in Murine Models of Dermal and Pulmonary Inflammation. *J. Immunol.* **2016**, *197*, 2421–2433.
- (15) Coll, R. C.; Hill, J. R.; Day, C. J.; Zamoshnikova, A.; Boucher, D.; Massey, N. L.; Chitty, J. L.; Fraser, J. A.; Jennings, M. P.; Robertson, A. A. B.; Schroder, K. MCC950 Directly Targets the NLRP3 ATP-Hydrolysis Motif for Inflammasome Inhibition. *Nat. Chem. Biol.* **2019**, *15*, 556–559.
- (16) vande Walle, L.; Stowe, I. B.; Šácha, P.; Lee, B. L.; Demon, D.; Fossoul, A.; van Hauwermeiren, F.; Saavedra, P. H. V.; Šimon, P.; Šubrt, V.; Kostka, L.; Stivala, C. E.; Pham, V. C.; Staben, S. T.; Yamazoe, S.; Konvalinka, J.; Kayagaki, N.; Lamkanfi, M. MCC950/CRID3 Potently Targets the NACHT Domain of Wild-Type NLRP3 but Not Disease-Associated Mutants for Inflammasome Inhibition. *PLoS Biol.* **2019**, *17*, No. e3000354.
- (17) Hochheiser, I.; Pilsl, M.; Hagelueken, G.; Moecking, J.; Marleaux, M.; Brinkschulte, R.; Latz, E.; Engel, C.; Geyer, M. Structure of the NLRP3 Decamer Bound to the Cytokine Release Inhibitor CRID3. *Nature* **2022**, *604*, 184–189.
- (18) Tapia-Abellán, A.; Angosto-Bazarra, D.; Martínez-Banaclocha, H.; de Torre-Minguela, C.; Cerón-Carrasco, J. P.; Pérez-Sánchez, H.; Arostegui, J. I.; Pelegrín, P. MCC950 closes the active conformation of NLRP3 to an inactive state. *Nat. Chem. Biol.* **2019**, *15*, 560–564.
- (19) Ohto, U.; Kamitsukasa, Y.; Ishida, H.; Zhang, Z.; Murakami, K.; Hirama, C.; Maekawa, S.; Shimizu, T. Structural basis for the oligomerization-mediated regulation of NLRP3 inflammasome activation. *Proc. Natl. Acad. Sci. U. S. A.* **2022**, *119*, No. e2121353119.
- (20) Shah, F.; Leung, L.; Barton, H. A.; Will, Y.; Rodrigues, A. D.; Greene, N.; Aleo, M. D. Setting Clinical Exposure Levels of Concern for Drug-Induced Liver Injury (DILI) Using Mechanistic in Vitro Assays. *Toxicol. Sci.* **2015**, *147*, 500–514.
- (21) Chen, M.; Borlak, J.; Tong, W. High Lipophilicity and High Daily Dose of Oral Medications Are Associated with Significant Risk for Drug-Induced Liver Injury. *Hepatology* **2013**, *58*, 388–396.
- (22) Hopkins, A. L.; Keserü, G. M.; Leeson, P. D.; Rees, D. C.; Reynolds, C. H. The Role of Ligand Efficiency Metrics in Drug Discovery. *Nat. Rev. Drug Discovery* **2014**, *13*, 105–121.
- (23) Zhang, K. E.; Naue, J. A.; Arison, B.; Vyas, K. P. Microsomal Metabolism of the 5-Lipoxygenase Inhibitor L-739,010: Evidence for Furan Bioactivation. *Chem. Res. Toxicol.* **1996**, *9*, 547–554.
- (24) Daudon, M.; Frochot, V.; Bazin, D.; Jungers, P. Drug-Induced Kidney Stones and Crystalline Nephropathy: Pathophysiology, Prevention and Treatment. *Drugs* **2018**, *78*, 163–201.
- (25) Wang, X.; Barbosa, J.; Blomgren, P.; Bremer, M. C.; Chen, J.; Crawford, J. J.; Deng, W.; Dong, L.; Eigenbrot, C.; Gallion, S.; Hau, J.; Hu, H.; Johnson, A. R.; Katewa, A.; Kropf, J. E.; Lee, S. H.; Liu, L.; Lubach, J. W.; Macaluso, J.; Maciejewski, P.; Mitchell, S. A.; Ortwinne, D. F.; Di Paolo, J.; Reif, K.; Scheerens, H.; Schmitt, A.; Wong, H.; Xiong, J.-M.; Xu, J.; Zhao, Z.; Zhou, F.; Currie, K. S.; Young, W. B. Discovery of Potent and Selective Tricyclic Inhibitors of Bruton's Tyrosine Kinase with Improved Druglike Properties. *ACS Med. Chem. Lett.* **2017**, *8*, 608–613.
- (26) Aliagas, I.; Gobbi, A.; Lee, M.-L.; Sellers, B. D. Comparison of LogP and LogD correction models trained with public and proprietary data sets. *J. Comput.-Aided Mol. Des.* **2022**, *36*, 253–262.
- (27) Stafford, J. A.; Veal, J. M.; Trzoss, L. L.; McBride, C. Chemical Compounds as Inhibitors of Interlukin-1 Activity. PCT WO2018/136890 A1.
- (28) Chen, E. C.; Broccatelli, F.; Plise, E.; Chen, B.; Liu, L.; Cheong, J.; Zhang, S.; Jorski, J.; Gaffney, K.; Umemoto, K. K.; Salphati, L. Evaluating the Utility of Canine Mdr1 Knockout Madin-Darby Canine Kidney I Cells in Permeability Screening and Efflux Substrate Determination. *Mol. Pharmaceutics* **2018**, *15*, 5103–5113.
- (29) Weekley, L. B.; Deldar, A.; Tapp, E. Development of renal function tests for measurement of urine concentrating ability, urine acidification, and glomerular filtration rate in female cynomolgus monkeys. *Contemp. Top. Lab. Anim. Sci.* **2003**, *42*, 22–25.
- (30) Sharif, H.; Wang, L.; Wang, W. L.; Magupalli, V. G.; Andreeva, L.; Qiao, Q.; Hauenstein, A.; Wu, Z.; Núñez, G.; Mao, Y.; Wu, H. Structural Mechanism for NEK7-Licensed Activation of NLRP3 Inflammasome. *Nature* **2019**, *570*, 338–343.
- (31) Andreeva, L.; David, L.; Rawson, S.; Shen, C.; Pasricha, T.; Pelegrin, P.; Wu, H. NLRP3 cages revealed by full-length mouse NLRP3 structure control pathway activation. *Cell* **2021**, *184*, 6299.e22–6312.e22.
- (32) Dekker, C.; Mattes, H.; Wright, M.; Boettcher, A.; Hinniger, A.; Hughes, N.; Kapps-Fouthier, S.; Eder, J.; Erbel, P.; Stiefl, N.; Mackay, A.; Farady, C. J. Crystal Structure of NLRP3 NACHT Domain With an Inhibitor Defines Mechanism of Inflammasome Inhibition. *J. Mol. Biol.* **2021**, *453*, No. 167309.
- (33) See [Supplemental Information](#).
- (34) We rely on MWB data as we were unable to develop a reliable rat whole blood assay.
- (35) Boxenbaum, H. Interspecies Scaling, Allometry, Physiological Time, and the Ground Plan of Pharmacokinetics. *J. Pharmacokinet. Biopharm.* **1982**, *10*, 201–227.
- (36) For a discussion of alternative methods of predicting human dose see: Peters, S. H.; Petersson, C.; Blaukat, A.; Halle, J.-P.; Dolgos, H. Prediction of active human dose: learnings from 20 years of Merck KGaA experience, illustrated by case studies. *Drug Discovery* **2020**, *25*, 909–919.
- (37) For an additional discussion of alternative methods of predicting human dose see: Davies, M.; Jones, R. D. O.; Grime, K.; Jansson-Löfmark, R.; Fretland, A. J.; Winiwarter, S.; Morgan, P.;

McGinnity, D. F. Improving the Accuracy of Predicted Human Pharmacokinetics: Lessons Learned from the AstraZeneca Drug Pipeline Over Two Decades. *Trends Pharmacol. Sci.* **2020**, *41*, 390–408.

(38) Rajamäki, K.; Lappalainen, J.; Oörni, K.; Välimäki, E.; Matikainen, S.; Kovánen, P. T.; Eklund, K. K. Cholesterol crystals activate the NLRP3 inflammasome in human macrophages: a novel link between cholesterol metabolism and inflammation. *PLoS One* **2010**, *5*, No. e11765.